ACS OMEGA
http://pubs.acs.org/journal/acsodf
Article

Facile Fabrication and Characterization of Amine-Functional Silica Coated Magnetic Iron Oxide Nanoparticles for Aqueous Carbon Dioxide Adsorption

Md. Muhyminul Islam, Md. Abdur Rahman,* Md. Ashraful Alam,* Md. Mahbubor Rahman, O. Thompson Mefford, Anwar Ul-Hamid, Jalil Miah, and Hasan Ahmad

Cite This: *ACS Omega* 2024, 9, 20891−20905

ABSTRACT: Surface active amine-functionalized silica coated magnetic iron oxide nanoparticles were prepared by a simple two-step process for adsorbing CO_2 gas from aqueous medium. First, oleic acid (OA) coated iron oxide magnetic particles (denoted as Fe_3O_4-OA) were prepared by a simple coprecipitation method. Then, the surface of the Fe_3O_4-OA particles was coated with silica by using tetraethyl orthosilicate. Finally, aminated Fe_3O_4/SiO_2-NH_2 nanoparticles were concomitantly formed by the reactions of 3-aminopropyl triethoxysilane with silica-coated particles. The formation of materials was confirmed by Fourier transform infrared spectral analysis. Transmission electron microscopic analysis revealed both spherical and needle-shaped morphologies of magnetic Fe_3O_4/SiO_2-NH_2 particles with an average size of 15 and 68.6 nm, respectively. The saturation magnetization of Fe_3O_4/SiO_2-NH_2 nanoparticles was found to be 33.6 emu g^{-1}, measured by a vibrating sample magnetometer at ambient conditions. The crystallinity and average crystallite size (7.0 nm) of the Fe_3O_4/SiO_2-NH_2 particles were revealed from X-ray diffraction data analyses. Thermogravimetric analysis exhibited good thermal stability of the nanoadsorbent up to an elevated temperature. Zeta potential measurements revealed pH-sensitive surface activity of Fe_3O_4/SiO_2-NH_2 nanoparticles in aqueous medium. The produced magnetic Fe_3O_4/SiO_2-NH_2 nanoparticles also exhibited efficient proton capturing activity (92%). The particles were used for magnetically recyclable adsorption of aqueous CO_2 at different pH values and temperatures. Fe_3O_4/SiO_2-NH_2 nanoparticles demonstrated the highest aqueous CO_2 adsorption efficiency (90%) at 40 °C, which is clearly two times higher than that of nonfunctionalized Fe_3O_4-OA particles.

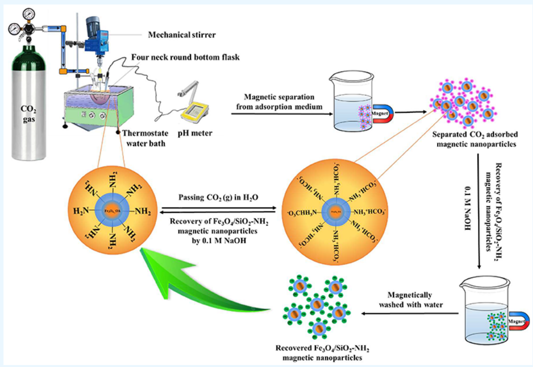

1. INTRODUCTION

Global warming is a major concern and has also been the greatest threat to all living species and their safe survival on earth. This is gradually increasing due to unplanned industrialization, urbanization, deforestation, and excessive and abusive use of the grazing fields that are increasing the emissions of CO_2 to the atmosphere.[1,2] Recently, the National Oceanic and Atmospheric Administration's (NOAA) worldwide monitoring laboratories have reported that the concentration of global average atmospheric CO_2 has reached 414.72 ppm (ppm).[3] In fact, the annual rate of increase in atmospheric CO_2 over the previous 60 years is around 100 times greater than that of the earlier usual increments.[3] This increased concentration of CO_2 in the atmosphere causes a net air-to-seawater CO_2 flux and a crucial threat to human health, animals, and even aquatic life, as it also decreases the concentration of dissolved oxygen in seawater. Additionally, the excessive concentration of CO_2 reduces tropical fish's aerobic performance.[4] It also causes significant tissue damage in vital organs like the liver, kidney, pancreas, and even the eyes.[5] With the emissions of CO_2 from fossil fuels, such as coal, mineral oil, and natural gas combustion for transportation, power production, and industries, both ecological and environmental conditions are becoming worse day-to-day.[7]

Thousands of scientists have been working to find environmentally benign, user-friendly, and cost-effective methods for decarbonization to mitigate CO_2 emissions in the atmosphere throughout the globe. Among other techniques reported for mitigation of CO_2 emission, bicarbonate ion formation in large scale via direct interactions between CO_2 and water is an important and easily accessible method. However, this process generates an acidic mixture that can

Received: December 17, 2023
Revised: April 18, 2024
Accepted: April 22, 2024
Published: May 2, 2024

https://doi.org/10.1021/acsomega.3c10082
ACS Omega 2024, 9, 20891−20905

cause a serious corrosion problem. Additionally, CO_2 conversion is also a major concern for catalytic processes, as it reduces the lifetime of reactor vessels as well as dramatically decreases the activity of catalysts within a very short time. Therefore, the industrial process can degrade the quality of equipment and the finished goods.[6] To minimize the emissions of CO_2, several other methods, such as precombustion, postcombustion, and oxyfuel combustion technologies have been applied in industries.[8−10] However, these methods are generally rather expensive, accounting around for 70 to 80% of the entire cost of the carbon capturing and sequestration technology.[11] The widely used postcombustion capture techniques include cryogenic separation, membrane separation, solvent absorption, and surface adsorption using various solid adsorbents.[12−16]

The adsorption method is more important than other techniques because it is reversible in nature, and the adsorption efficiency can be easily improved by modifying the structure and functionality of the adsorbent materials. The CO_2 adsorption efficiency can, therefore, be improved by selecting an appropriately designed adsorbent material though solid adsorbents, like ordered porous carbon, activated carbon fibers, natural products derived porous carbon, activated carbon, and graphene, or noncarbonated adsorbents, such as silica, zeolites, porous polymers and their membranes, metal organic frameworks, alkali metal-based materials, and metal oxide carbonates, have some advantages over other adsorbent material, for example, ease of handling, required low regeneration energy, low cost, high capacity for adsorption, and relatively faster adsorption−desorption kinetics. These methods are partially discouraged due to their certain limitations, such as renewal and recyclability issues, high-temperature reactions, and complex procedures.[17−19]

Application of suitable basic solvents is another important strategy for the absorption of CO_2. Having various advantages, such as high absorption efficiency, high desorption capability, and low regeneration energy, many basic solvents, such as salts of aqueous amines, ionic liquids, piperazine and their derivatives, and amino alcohols, are being used for CO_2 absorption. However, these solvents have some disadvantages, like undesirable solvent loss,[20] high energy consumption,[21,22] formation of unwanted byproducts,[23] and corrosion problems.[24] Besides these base solvents, water has many advantages, such as inert nature, low vapor pressure, the highest specific heat capacity, inexpensiveness, easy availability, nontoxicity, noncorrosiveness, and inflammability, and it is attracting much attention from researchers. For example, Pineda et al. evaluated CO_2 absorption using methanol-based nanofluids of SiO_2 in an acrylic tray column absorber and concluded that SiO_2 nanofluids enhanced CO_2 capture by 9.7%.[25] Kim et al. investigated the CO_2 absorption properties of water-based SiO_2 nanofluids. They reported that the CO_2 absorption rate of the water-based SiO_2 nanofluid was increased up to 24%.[26] In an absorption packed column, J. Salimi et al. investigated the CO_2 absorption by water-based Al_2O_3 and Al_2O_3-SiO_2 nanofluids. According to their results Al_2O_3 nanofluid markedly increased the absorption capacity (14%) compared to that of Al_2O_3-SiO_2 (10%) nanofluid.[27]

Recently metal oxide nanoparticles have received considerable research interest because of their unique behaviors, namely rapid rate of recovery, low toxicity, large active surface area, magnetic manipulation, and reusability potentials.[1,28−31] For example, Haghtalab et al. utilized ZnO and SiO_2 nanofluids to evaluate CO_2 absorption in a bubble absorber. They found that the presence of ZnO in the medium raised the CO_2 capturing efficiency up to 14% compared to that of SiO_2 (7%).[32] Samadi et al. demonstrated the effect of magnetic properties on CO_2/water absorption. The ability of nanosolutions for absorbing CO_2 can be increased up to 22.35% compared to that in the absence of any magnetic field.[33] Salimi et al. studied the CO_2 absorption of water-based Fe_3O_4 and NiO nanofluids and reported that the absorption amount by Fe_3O_4 nanofluid was 12%, which is higher than that of NiO (9.5%).[34] Rahmatmand et al. investigated CO_2 absorption with water-based Al_2O_3, carbon nanotubes, SiO_2, and Fe_3O_4 nanofluids in a high-pressure batch system. In this study, Al_2O_3, SiO_2, Fe_3O_4, and carbon nanotube nanoparticles increased CO_2 absorption capacity in pure water by 18%, 21%, 24%, and 34%, respectively.[35]

Several studies have demonstrated that the adsorption of CO_2 involves formation of chemical bonding between gaseous CO_2 and the amino groups present on the surface of magnetic particles.[36,37] To facilitate this adsorption process, several nanofluids were prepared by using a probe-type ultrasonic agitator. For example, Elhambakhsh et al. studied the effect of the number of primary amine (-NH_2) groups on the adsorption of CO_2 in base solvent with water. In their study, they synthesized aminated silica coated magnetic particles (Fe_3O_4@SiO_2-AP) and carboxyl-aminated silica coated magnetic particles (Fe_3O_4@SiO_2-lysine). The adsorption efficiency of Fe_3O_4@SiO_2-lysine particles was 88.00%, which is higher than that of Fe_3O_4@SiO_2-AP particles. They proved that the higher the number of amine groups, the higher the adsorption of CO_2.[36] In another work, Elhambakhsh et al. studied the adsorption of CO_2 by Fe_3O_4, Fe_3O_4-pyroline, Fe_3O_4-lysine, and Fe_3O_4@SiO_2-NH_2 nanoparticles in the base solvent sulfinol-M considering various aspects. They mainly focused on the stability of the particles at higher concentrations, chemical reactions between the particles and CO_2, etc. They reported that all the Fe_3O_4 nanoparticles modified with amine functional groups are stable at higher concentrations. The reaction tendency among such particles and CO_2 molecules was higher, and the highest adsorption efficiency was noticed.[37] Fe_3O_4@SiO_2-SNH_2 nanoparticles were synthesized by the functionalization of Fe_3O_4 using tetraethyl orthosilicate, aminopropyl triethoxysilane, and diethylene tetraamine (DETA). The obtained adsorbent particles were used to capture CO_2 in a base solvent by Arshadi et al.[24] Their absorption mechanism was based on the size decreasing of CO_2 bubbles by the -NH_2 groups of the synthesized particles. They considered the net effects of nanoparticle loading, hydrophilicity, the quantity of nanoparticles, reaction temperature, and absorption time for CO_2 absorption. In this research, they devised a customized bubble-based column system, where a gas mixture containing CO_2 was introduced into the column in the form of small bubbles. This was achieved by employing a gas diffuser with a pore size ranging from 4 to 10 μm, which was positioned at the column's basement. Then, the diffusion boundary layer of the CO_2 bubbles is more quickly surrounded by the symmetric amine-based nanodendric adsorbent, creating a symmetrical interface that is stabilized by CO_2 on the solid surface. The efficiency of CO_2 absorption was found to be the highest when using an absorbent with a high density of amine functional sites and high hydrophilicity, resulting in about 70% enhancement in CO_2 absorption. The size classification of these gas bubbles has

https://doi.org/10.1021/acsomega.3c10082
ACS Omega 2024, 9, 20891−20905

Scheme 1. Schematic Representation of the Synthesis of Amine-Functionalized Silica Coated Iron Oxide Magnetic Nanoparticles

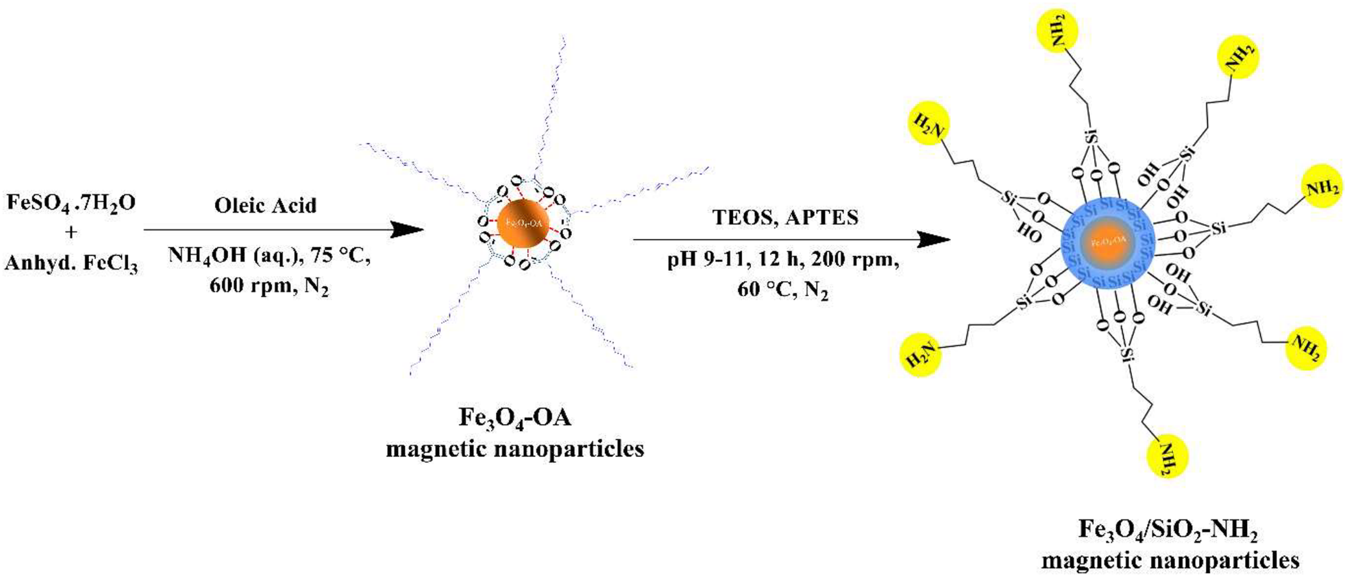

a significant impact on the efficiency of CO_2 absorption. However, it is well-known that the size of the gas bubbles in a bubble column is influenced by several factors, such as interfacial tension, gas-phase density, liquid-phase viscosity, pressure, temperature, and orifice diameter. A study of CO_2 absorption based on CO_2 solubility in water was conducted by Hafizi et al. using their prepared DETA functionalized Fe_3O_4 nanoparticles. The absorption efficiency was about 77%.[38] Oddo et al. also investigated the influence of temperature on CO_2 absorption using aminated magnetic nanoparticles.[39] These research works overlooked the pH changes in their dispersion medium, distilled water, which is a crucial parameter for affecting the CO_2 capture. This is because CO_2 molecules easily form carbonic acid in water due to the Lewis acidic characteristic, and the carbonic acid molecules dissociate to become bicarbonate ions. Additionally, these studies did not consider the alkaline properties of their used solvents and that may contain water, which facilitates CO_2 capture through acid−base interactions. These characteristics may hamper the capacity and rates of CO_2 absorption.

In our previous investigation, we developed potentially active difunctional core−shell composite polymer particles and used them as a recyclable adsorbent for capturing acidic CO_2 in an aqueous medium.[40] This research endeavor provided valuable insights into the applicability of composite polymer particles for CO_2 capturing; however, several significant limitations were identified. One of the major drawbacks of our previous approach was the intricate and time-consuming multistep synthesis process required to fabricate the composite polymer particles. Another critical limitation is the gradual dissolution of the copolymer-shell layer in the aqueous medium and the requirement of prolonged mechanical separation procedures. Furthermore, the composite polymer particles lacked the ability to undergo efficient regeneration after CO_2 adsorption−desorption cycles from the dispersion medium. The lack of renderability raised concerns regarding the long-term sustainability and cost-effectiveness of the CO_2 capturing process.[30,37,39] Therefore, appropriate design and synthesis of adsorbent materials having faster adsorption−desorption kinetics, considerable recyclability, and promising colloidal dispersity with rapid real-time separation capability from the dispersion medium are highly crucial for low-cost adsorption of CO_2.

Therefore, the objective of this research work is the design and synthesis of amine-functionalized silica-coated surface-active magnetic iron oxide particles via a facile two-step process for magnetically recyclable, economically feasible, and faster adsorption of CO_2 from an aqueous medium at different conditions. Here, magnetic iron oxide nanoparticles ensure suitable magnetism that allows relatively easier and faster separation of the adsorbent materials from the dispersion medium via magnetic attraction by using a simple permanent magnet. However, bare magnetic nanoparticles are highly prone to aggregate from the dispersion medium. Usually magnetic particles cannot be redispersed even after removal of the magnetic field because of their self-magnetism, high surface energy, and high ratio of surface area-to-volume. Optimum silica coating on the bare-surface of iron oxide particles works as a self-defensive compartment for each magnetic-core. Silica coating also improved magnetism via enhancing the number of net unpaired electron spin-order structures. Additionally, silica coating also enhances dispersity, colloidal stability, and hydrophilicity and minimizes the possibility of particles' flocculation and leaching out of iron atoms from core particles during multiple adsorption−desorption cycles of CO_2 in acidic medium. Amine functionalization of the silica coated magnetic iron oxide adsorbent particles provides an active cationic surface via easier protonation in aqueous medium to adsorb aqueous CO_2 as bicarbonate ions. The continuous pH changes for the adsorption/desorption of CO_2 in the presence of adsorbent particles in the blank medium, namely distilled deionized water, were assessed and monitored by using a simple magnet and a pH meter. The synthesized particles were used to capture CO_2 under various conditions via using a highly accessible aqueous medium. Finally, the magnetically recyclable adsorption−desorption efficiency of aqueous CO_2 of the designed nanoparticles was also studied.

https://doi.org/10.1021/acsomega.3c10082
ACS Omega 2024, 9, 20891−20905

2. EXPERIMENTAL SECTION

2.1. Materials. Iron(III) chloride ($FeCl_3$), iron(II) sulfate heptahydrate ($FeSO_4 \cdot 7H_2O$), ammonium hydroxide (25%, w/v), and ethanol were purchased from Merck, Germany. Tetraethyl orthosilicate (TEOS) and oleic acid (OA) were purchased from Sigma-Aldrich, Chemie GmbH, USA, and 3-aminopropyl triethoxysilane was purchased from Tokyo Chemical Industry Co., Ltd., Japan. CO_2 used for adsorption was purchased from Qingdao Guida Special Gas Company Ltd., China. All other chemicals were of analytical grade and used without further purification. Distilled deionized water was used throughout the study.

2.2. Methods. *2.2.1. Synthesis of Oleic Acid Coated Fe_3O_4 Magnetic Nanoparticles.* Oleic acid-coated iron oxide magnetic (Fe_3O_4-OA) nanoparticles were synthesized by the modified coprecipitation method[41,42] using anhydrous $FeCl_3$ and $FeSO_4 \cdot 7H_2O$ salts with a Fe^{3+}/Fe^{2+} molar ratio of 2:1, which is shown in the first part of the Scheme 1. The detail recipes are shown in Table S1. In brief, under purging nitrogen, suitable amounts of $FeCl_3$ and $FeSO_4 \cdot 7H_2O$ salts were dissolved in distilled deionized water, the solution was transferred into a 500 mL three-necked round-bottom flask, and the flask was placed on a thermostat oil bath. The mixture was mechanically stirred continuously at 600 rpm. The reactor flask was heated at 80 °C for 20 min, followed by dropwise addition of aqueous ammonia solution until the pH of the reaction mixture reached between 9 and 10. A black precipitate was formed immediately just after complete addition of aqueous NH_4OH. After 30 min of reaction, a considerable amount of oleic acid was added and the reaction mixture was stirred for another 30 min at the same temperature. Finally, the dispersion was magnetically washed several times with 0.01 M HCl and with distilled water. The obtained solid mass was dried in an electric oven at 80 °C and stored in a black-tape wrapped container, which was kept in a refrigerator for further use.

2.2.2. Surface Coating of Magnetic Fe_3O_4-OA Nanoparticles with Amine-Functional Silica. The in situ amine-functionalization and silica coating protocol of magnetic Fe_3O_4-OA nanoparticles is shown in the second step of Scheme 1. The variable ingredients and recipes for synthesizing Fe_3O_4/SiO_2-NH_2 nanoparticles are shown in Table S2. In brief, Fe_3O_4-OA particles was dispersed ultrasonically in a conical flask containing distilled deionized water and ethanol. The dispersion was, then, treated with aqueous NH_3 (25 wt %) solution to maintain the dispersion pH at 9−11. Afterward, the mixture was magnetically stirred for 1 h at 200 rpm. Then, the required amount of TEOS was added to the system. After 6 h, the necessary amount of APTES was added to the stirred dispersion. The dispersion was magnetically stirred under nitrogen at identical conditions, and the reaction was continued for 6 h. The nanoparticles from the reaction mixture were, then, collected by using an external magnet and magnetically washed five times with deionized distilled water. The washed particles were dried in an electric oven at 60 °C and stored in a refrigerator for real application.

2.2.3. Characterization of Amine-Functionalized Silica Coated Magnetic Nanoparticles. The physicochemical characteristics of reference Fe_3O_4-OA and Fe_3O_4/SiO_2-NH_2 were studied through various techniques to get insight on the functional groups, thermal stability, saturation magnetization, morphology, and crystalline structure of Fe_3O_4-OA, before and after the functionalization process. These techniques were Fourier transform infrared spectroscopy (FTIR), which was conducted using a PerkinElmer FTIR-100 spectrophotometer, Waltham, MA, USA. Prior to the analytical measurements, the sample dispersion underwent a purification process and was subsequently dried at 60 °C overnight and vacuum-dried under reduced pressure in a desiccator. About 10 mg of the dried sample was added to 100 mg of vacuum-dried KBr-pellets to make a thin disk using a high-pressure compressor at room temperature. The spectral data were acquired by scanning across a wavelength range of 4000 to 200 cm^{-1} in transmission mode. Thermal analyses were performed using a thermogravimetric analyzer, Seiko Instrument Inc., EXSTAR-6000, Japan. The thermal properties of the dry powdered samples were evaluated at a thermal range of 30 to 800 °C using a heating rate of 10 °C per minute under nitrogen atmosphere. The initial weight of each sample was approximately 10 mg. During this experiment the continuous weight loss was recorded against changing temperature. Magnetization measurements were performed at 300 K using a vibrating sample magnetometer (VSM), MicroSense, EV9, USA. VSM analysis was conducted over a magnetic field range of ±50,000 Oe. In this experiment, dried powdered samples were utilized. Each sample had an initial weight of around 10 mg. X-ray diffraction analysis of the nanoparticles was performed using an X-ray diffractometer, Bruker D8 Advance, Germany. Monochromatic CuKα radiation ($\lambda \approx 1.5418$ Å) was utilized, with a tube voltage of 40 kV and a tube current of 40 mA, at room temperature. The diffraction scans covered a 2θ range from 10 to 80°, employing a continuous scan rate of 0.167° per minute, with the position-sensitive detector aperture set to enhance resolution. Transmission electron microscopy (TEM), Hitachi HT7830, Japan, measurements were performed at 120 kV. To make samples for the TEM experiment, the diluted dispersion of each sample was dropped on a Cu-grid using a micropipette. The sample containing grid was then dried in a vacuum desiccator overnight under reduced pressure at room temperature. The dried sample surface was finally coated with Au using a vacuum sputtering machine. Prior to TEM observation the metal-coated Cu-grids were preserved in a vacuum desiccator at dark. A centrifuge machine, Kokuson Corporation, Tokyo, Japan, pH meter, MP220, Mettler Toledo, Switzerland, and hot plate magnetic starrier, DLAB, from China, were also used. The zeta potential of synthesized nanoparticles was determined using a ZS-100 Nano Particle Analyzer, Malvern, USA, by dispersing the nanoparticles in deionized distilled water at various pH levels. The dispersion was diluted to approximately 0.01% of solid content using deionized distilled water, and the measurements were conducted at 25 °C.

2.2.4. Proton Capturing Activities of Fe_3O_4/SiO_2-NH_2 Nanoparticles. The proton capture efficiencies of Fe_3O_4/SiO_2-NH_2 and reference-Fe_3O_4-OA nanoparticles were measured via monitoring the pH variations of their aqueous dispersions at different sets of temperatures. The overall pH changes and individual change of the hydrogen ion concentration for specific points (pH 6 and pH 4) at different temperatures are shown in detail in Figure S1. In brief, the experiment was conducted using a four-necked round-bottomed flask, which was equipped in a thermostat water bath. 100 mL of deionized distilled water was added to the flask, and the temperature of the flask was adjusted to 25 °C. The initial pH of the water in the flask was set to 6, by adding

https://doi.org/10.1021/acsomega.3c10082
ACS Omega 2024, 9, 20891−20905

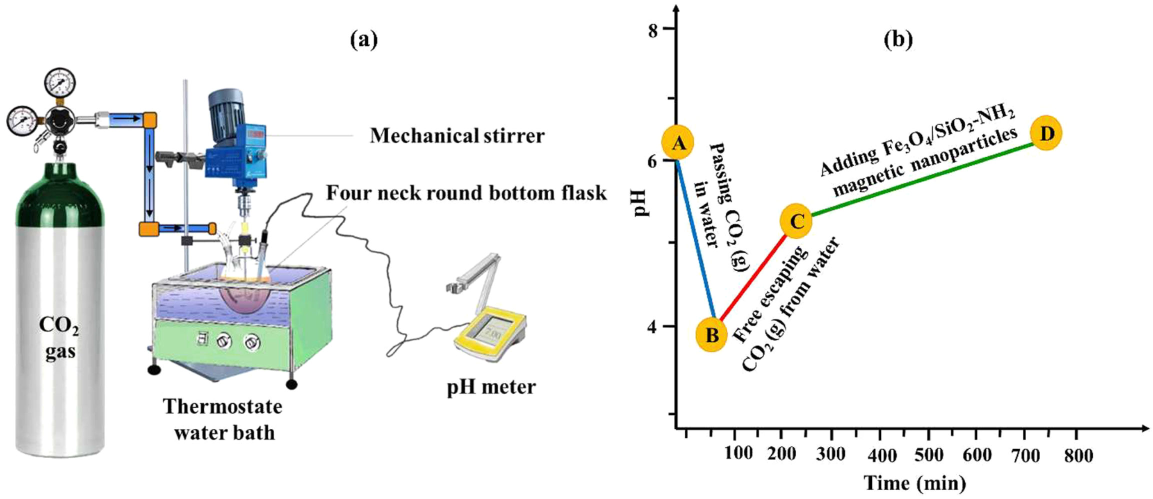

Figure 1. (a) A typical schematic experimental set up, and (b) graphical representation of the pH variations for the adsorption of aqueous CO_2 by magnetic Fe_3O_4/SiO_2-NH_2 nanoparticles.[40]

0.01 M HCl aqueous solution. Then, a certain amount of dry Fe_3O_4/SiO_2-NH_2 nanoparticles was introduced into the flask. The dispersion was mechanically stirred at 100 rpm, and its pH change was monitored over a period of 2 h. This identical experiment was also conducted for 30, 35, and 40 °C. All the measurements were repeated for three times, and their average values are reported with standard error bars. For both the Fe_3O_4/SiO_2-NH_2 and reference-Fe_3O_4-OA nanoparticles all these experiments were also conducted at pH 4. Observed changes in hydrogen ion concentration as well as pH-specific changes for all the experiments at different temperatures at typical pH values are graphically illustrated in Tables S3 and S4.

2.2.5. Experimental Setup for the Adsorption of Aqueous CO_2. An aqueous CO_2 absorption study was performed in a four-necked round bottomed flask according to our established procedure with some modifications, which is schematically shown in Figure 1.[40] Our real experimental set up used for aqueous adsorption of CO_2 is illustrated in Figure S2. The modified protocol for aqueous adsorption of CO_2 is described here in brief: a certain amount of distilled deionized water was taken in the flask. The pH of the water was initially adjusted to 6 (point A, Figure 1b) by using a few drops of dilute HCl solution, and CO_2 gas was started to pass into the flask from a cylinder (Figure 1a). During the passing of gaseous CO_2 in the host medium, namely distilled water, the pH change was monitored by using a simple pH meter. When the pH reached to point B, CO_2 gas passing was stopped. Then, to escape free CO_2 from the host medium, the pH change was observed for 2 h until it reached to point C (Figure 1b). At that point, a suitable amount of magnetic adsorbent nanoparticles was added to the CO_2 consumed aqueous medium. Finally, the pH of the dispersion was monitored continuously until the pH reached to the fixed-point D (Figure 1b).

2.2.6. Aqueous CO_2 Adsorption Efficiencies of Fe_3O_4/SiO_2-NH_2 and Reference-Fe_3O_4-OA Nanoparticles. The performance of synthesized magnetic nanoparticles was assessed for adsorption of CO_2 by using deionized distilled water as a host medium at different pH values and temperatures. At each temperature, initially the pH value of 100 mL of distilled water was fixed at 6 (point A in Figure 1b) using dilute HCl, and then, this pH value was reduced to 4 (fixed at point B) by passing CO_2 gas from the cylinder. CO_2 passing was then stopped until the pH value became constant at a higher pH value (at point C), allowing a stable pH through the free escaping of undissolved CO_2. At this stage (point C), a suitable quantity of adsorbent nanoparticles was added, and we had to wait until the pH value of the dispersion reached to the highest value (point D). At each stage (points A to D) mechanical stirring was kept continuous at 100 rpm. The difference in the molar hydrogen ion concentration between points D and C was used to calculate the captured amount of CO_2 by experimental nanoparticles using the logarithmic relationship which is shown in eq 1. The trends in the change of pH values, and their individual values, with hydrogen ion concentrations for each measurement are illustrated in Figures S3 and S4 and in Tables S5, S6, and S7, respectively.

$$\text{pH} = -\log\,[\text{H}^+] \tag{1}$$

The percentage efficiency for aqueous CO_2 adsorption was calculated by using eq 2.

$$\begin{aligned} &\text{CO}_2 \text{ adsorption efficiency (\%)} \\ &\quad = (\text{Amount of adsorbed CO}_2 \text{ at point C} \\ &\qquad - \text{Amount of adsorbed CO}_2 \text{ at point D})/ \\ &\qquad (\text{Amount of adsorbed CO}_2 \text{ at point C}) \times 100 \end{aligned} \tag{2}$$

2.2.7. Recovery and Reuses of CO_2-Adsorbed Magnetic Fe_3O_4/SiO_2-NH_2 Nanoparticles. This investigation involves five cycles of CO_2 adsorption and desorption at 40 °C by using a simple permanent magnet and 0.01 g of magnetic Fe_3O_4/SiO_2-NH_2 nanoparticles in aqueous medium. Gas-adsorbed Fe_3O_4/SiO_2-NH_2 nanoparticles were magnetically separated from the aqueous dispersion. Then, the CO_2 gas-bounded adsorbent was treated with 0.1 M aqueous NaOH solution to free the adsorbent nanoparticles via formation of the consumed CO_2 gas as a solid product, namely $NaHCO_3$(*s*). After that, the freed adsorbent nanoparticles were magnetically separated, washed with distilled deionized water, and reused for the next cycle of CO_2 adsorption. The recovery and reuse of adsorbent nanomaterials were studied up to the fifth cycle.

https://doi.org/10.1021/acsomega.3c10082
ACS Omega 2024, 9, 20891−20905

3. RESULTS AND DISCUSSION

3.1. Formation and Functionality of Fe_3O_4/SiO_2-NH_2 Nanoparticles. The formation of magnetic iron oxide, OA-capping, and aminated-silica coating on the bare surface of magnetic nanoparticles were confirmed by FTIR spectra analyses, which are shown in Figure 2. In the FTIR spectrum of Fe_3O_4-OA (Figure 2a), a typical broad peak appearing at 3200−3700 cm^{-1} is due to the -O−H stretching modes of hydrophobically capped-OA and physiochemically adsorbed water on the surface of magnetic particles.[43−45] The C−H stretching vibrations of unsaturated moieties were found at 3020−3170 cm^{-1}, while two other bands appeared at 2850 and 2922 cm^{-1}, that were assignable to the characteristic symmetric and asymmetric stretchings of C−H bonds in the -CH_2 and -CH_3 groups of OA. A quite broad band was seen at 1633 cm^{-1} because of the band overlapping of the stretching vibration mode of C═C and the bending vibration of O−H groups. The C═O stretching vibrations of carboxylate groups in OA appeared at relatively lower wavenumbers (1385 and 1408 cm^{-1}), due to the chelate formation via ligation to the Fe atoms on the surface of Fe_3O_4 nanoparticles.[45] In addition, the C−O stretching vibration band was seen at 1108 cm^{-1}, while two additional characteristic chain bending vibration peaks for C−C in long chained OA appeared 890 and 795 cm^{-1}. Two significant vibrational absorption signals were observed at 621 and 403 cm^{-1} that can be attributed to the Fe−O bonds in Fe_3O_4.[44] These bands revealed that the Fe_3O_4 nanoparticles were formed and their bare surface was capped with OA. In the FTIR spectrum of Fe_3O_4/SiO_2-NH_2, several peak positions, such as O−H, aliphatic and vinylic C−H, C═O, C−O, C−C, and Fe−O bands, were shifted (Figure 2b). In addition, some characteristic new vibrational peaks appeared in the regions of 1050−1100 cm^{-1} and 791−805 cm^{-1} that can be assignable to the asymmetric and symmetric stretching of Si−O and bridging Si−O−Si bonds, respectively.[46,47] The peak at 3400 cm^{-1} corresponded to the free N−H stretching, which was quite broad due to the overlapping with the O−H stretching, whereas the peak at 1630 cm^{-1} was assignable to the N−H bending vibration of -NH_2.[48] The symmetric and asymmetric C−H stretching vibrations of propyl groups were also observed at 2850 and 2925 cm^{-1}, respectively, whereas the bending vibrations of -CH_2 in the propyl chain appeared at 895 and 795 cm^{-1}.[49,50] At 1554 cm^{-1}, a deformation of the vibrational absorption peak of N−H bond occurred. These results suggested that the bare surface coated with silica and aminopropyl groups was concomitantly introduced on the surface of magnetic Fe_3O_4 nanoparticles.[51]

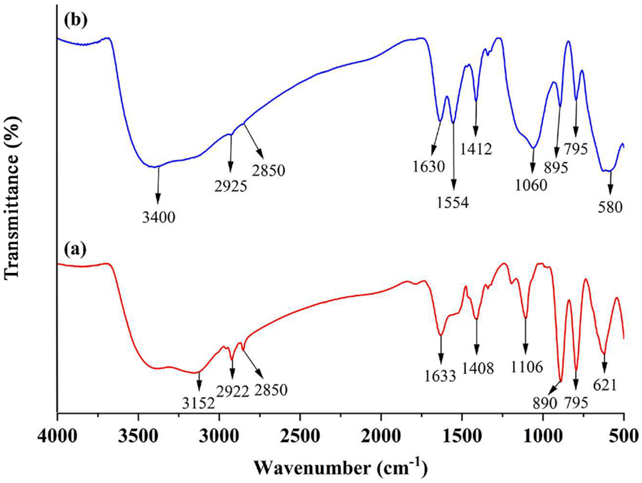

Figure 2. FTIR spectra of (a) reference-Fe_3O_4-OA and (b) Fe_3O_4/SiO_2-NH_2 magnetic nanoparticles.

3.2. Shape, Size, Surface Morphology, and Crystal Structure of Fe_3O_4/SiO_2-NH_2 Nanoparticles. TEM images of Fe_3O_4-OA particles are shown at different magnification scales in Figure 3a−c, which illustrate the alignment of tiny spherical particles with some needle-like rods with unsmooth surface morphology. The average length of the nanoneedles was around 63.82 nm, and they were about 9.80 nm wide. One can see that some Fe_3O_4-OA nanoparticles were spherical in shape with an average size of 8.77 nm. Such needle-shaped alignment has also been noticed for magnetic particles in previous reports.[52,53] Wang et al. reported that the formation of such a needle-shaped morphology is possible, when the crystal growth rate is relatively higher in the direction of a single plane of (110).[54] After surface coverage of Fe_3O_4-OA particles with an aminated SiO_2 layer, the TEM images at different magnification scales in Figure 3d−f showed the retention of their sizes in both spherical and needle-shaped particles.[55] However, their average sizes and surface

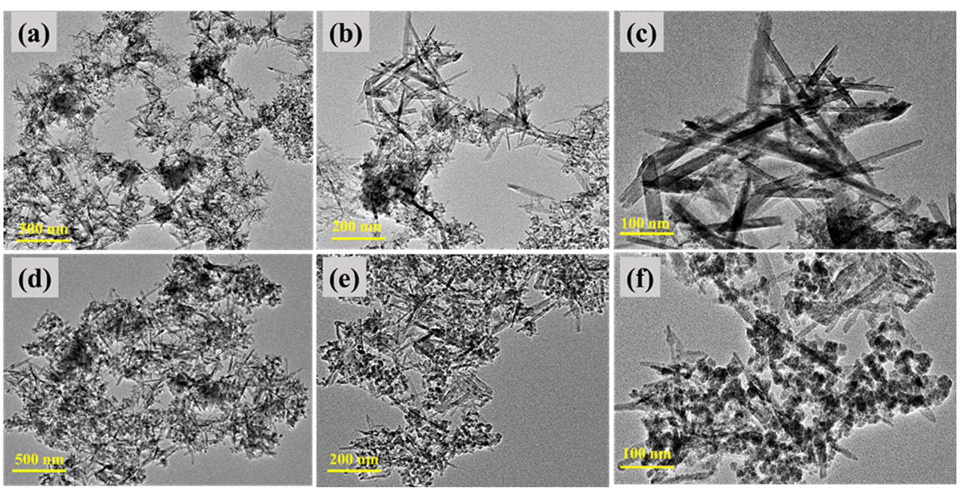

Figure 3. TEM images (a−c) of Fe_3O_4-OA and (d−f) for Fe_3O_4/SiO_2-NH_2 magnetic nanoparticles at different magnifications.

https://doi.org/10.1021/acsomega.3c10082
ACS Omega 2024, 9, 20891−20905

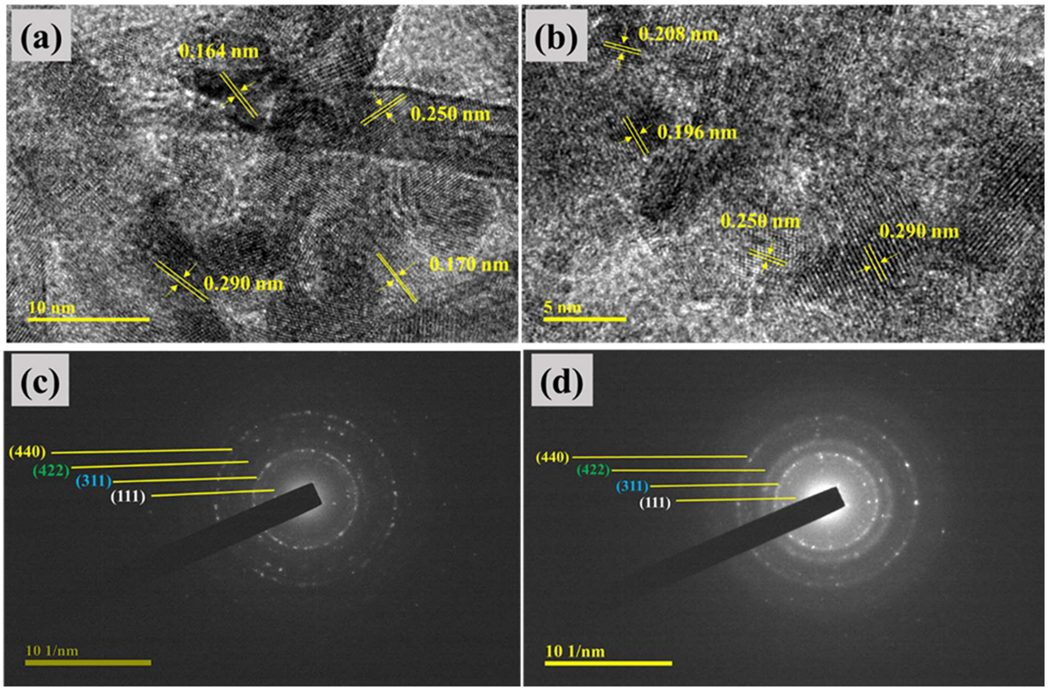

Figure 4. HRTEM images (a and b) and SAED patterns (c and d) of reference-Fe_3O_4-OA and Fe_3O_4/SiO_2-NH_2 magnetic nanoparticles, respectively.

morphologies were slightly changed because of the coating with amine functional hydrophilic silica. For example, the average size of spherical Fe_3O_4/SiO_2-NH_2 was found to be 10.04 nm and the needle-shaped particles were around 65.56 nm in length and about 10.50 nm in width. In addition, the needle-shaped alignment of tiny Fe_3O_4-OA particles was mostly preserved, as such an arrangement is quite evident during functionalization. The darker spots accounted for the aggregation of tiny iron oxide particles, while the less dense region around the darker spots represents the amorphous SiO_2 coating. The average sizes of both spherical and rod-shaped Fe_3O_4/SiO_2-NH_2 particles are fairly larger than those of Fe_3O_4-OA particles, which is an indication of successful surface modification with hydrophilic amine functional silica.

Representative high-resolution TEM (HRTEM) micrographs and selected area electron diffraction (SAED) patterns of Fe_3O_4-OA and Fe_3O_4/SiO_2-NH_2 nanocrystals are shown in Figure 4. In the HRTEM images of Fe_3O_4-OA (Figure 4a), the Braves lattice interplanar distances were measured to be about 0.290, 0.250, 0.170, and 0.164 nm, which can be assignable to the (220), (311), (422), and (511) crystalline planes of the Fe_3O_4 core, respectively.[56] Besides, a typical HRTEM micrograph of Fe_3O_4/SiO_2-NH_2 nanocrystals (Figure 4b) also exhibited vividly clear lattice fringes. The interplanar distances of Fe_3O_4/SiO_2-NH_2 nanoparticles were calculated to be 0.290, 0.250, 0.208, and 0.196 nm, which are assignable to the Braves lattice (220), (311), (400), and (331) planes. The lattice spacing of crystalline planes is almost similar to that of found in the XRD pattern, except for the (400) crystalline plane.[56,57] The selected area electron diffraction (SAED) patterns of both bare and silica coated nanoparticles (Figure 4c and d) depicted bright Debye−Scherrer rings, which indicate the polycrystalline nature of the Fe_3O_4 core as indicated by XRD patterns. The ring patterns corresponded to the (111), (220), (311), (422), and (440) planes.

The crystallinity and crystallite size of prepared nanoparticles were measured by X-ray diffraction (XRD). The XRD patterns of Fe_3O_4-OA and the effect of amine functionalization and silica coating on the crystal structure of Fe_3O_4-OA core particles are shown in Figure 5. The XRD pattern of Fe_3O_4-O_A

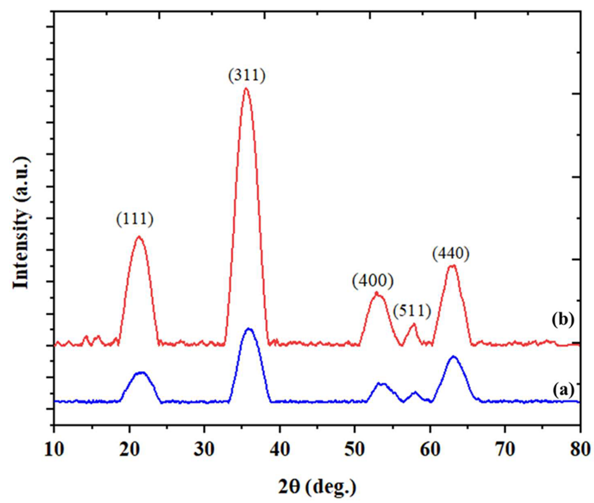

Figure 5. X-ray diffraction patterns of (a) Fe_3O_4-OA and (b) Fe_3O_4/SiO_2-NH_2 magnetic nanoparticles.

revealed five characteristic peaks at the two theta values of 21.11°, 35.5°, 53.36°, 57.37°, and 62.95°, which are assignable to the lattice planes of (111), (311), (422), (511), and (440), respectively (Figure 5a). The presence of these diffraction signals corresponds to the crystalline cubic spinal structure of Fe_3O_4 nanoparticles.[58−6061] In the XRD pattern of Fe_3O_4/SiO_2-NH_2 no additional peak was observable, which implied that the Fe_3O_4-OA crystal structure was not affected by amine functionalization and silica coating during the formation of

https://doi.org/10.1021/acsomega.3c10082
ACS Omega 2024, 9, 20891−20905

Fe_3O_4/SiO_2-NH_2 nanoparticles. In addition, no broad reflection was observable at the lower 2θ regions for both the particles because of minor amorphous segments of OA-capping (Figure 5a), and in the presence of optimum amorphous silica coating (Figure 5b).[58] The diffraction signal intensity of Fe_3O_4/SiO_2-NH_2 nanoparticles was relatively higher than that of Fe_3O_4-OA, which is demonstrating that the improvement in crystallinity is via optimum TEOS coated iron oxide nanoparticles. The broadening of each peak in both the XRD patterns is meant for the lower crystallite sizes that were calculated by using Scherrer's eq 3

$$D = K\lambda/\beta \cos\theta \qquad (3)$$

where D is the average diameter of each crystallite, K is the Scherrer constant, λ is the X-ray wavelength (0.15406 nm), β is the full-width at half-maximum of a peak, and θ is the Bragg's diffraction angle. Considering the most intense signal (311), the average crystallite size of reference Fe_3O_4-OA was calculated to be 8.13 nm, while for the aminated silica coated iron oxide it was 7.00 nm. Such crystallite size reductions for postsynthesis coated magnetic particles have already been noticed in previous literature.[62−64]

3.3. Magnetism of Fe_3O_4/SiO_2-NH_2 Nanoparticles. Figure 6 illustrates the magnetization curves of Fe_3O_4/SiO_2-NH_2 and reference Fe_3O_4-OA nanoparticles as a function of the applied magnetic field at ambient conditions. The existence of open hysteresis loops in their magnetization versus applied magnetic fields with very negligible remanence and coercivity was observed. The presence of linear hysteresis and minimal remanence and coercivity demonstrates the single domain, paramagnetism, and high crystallinity of these magnetic nanoparticles. The saturation magnetization (M_s) was calculated with respect to the mass of reference Fe_3O_4-OA. The M_s value of Fe_3O_4/SiO_2-NH_2 nanoparticles was slightly higher (33.61 emug^{-1}) than that of Fe_3O_4-OA particles (31.52 emug^{-1}). The increase in M_s value is because of the improvement in uniformity of the surface characteristics and net electron spin stabilization via chemical bonding with silanol moieties.[65] The lower magnetism of the Fe_3O_4-OA is due to a reduction in the number of oxygen atoms surrounding the octahedral iron, which is five rather than six as in the bulk magnetite. The in-plane oxygen ions are also closer to the Fe ions at the surface of magnetite, enhancing the hybridization of $d_{x^2-y^2}$ orbitals. As the orbitals move further from the Fermi level, they become partially empty, resulting in magnetic moment loss at the surface of the Fe_3O_4-OA nanoparticles.[66−68] In the absence of an external magnetic field, the Fe_3O_4/SiO_2-NH_2 particles are fully dispersible in aqueous medium. However, in the presence of a permanent magnet, the nanoparticles were completely separated from their aqueous dispersion within a few seconds (inset images shown in Figure 6). The exhibited magnetic behavior is suitable for faster separation of the adsorbent nanoparticles from their dispersion using a simple, easily accessible permanent magnet for multiple adsorption−desorption and recycling applications.

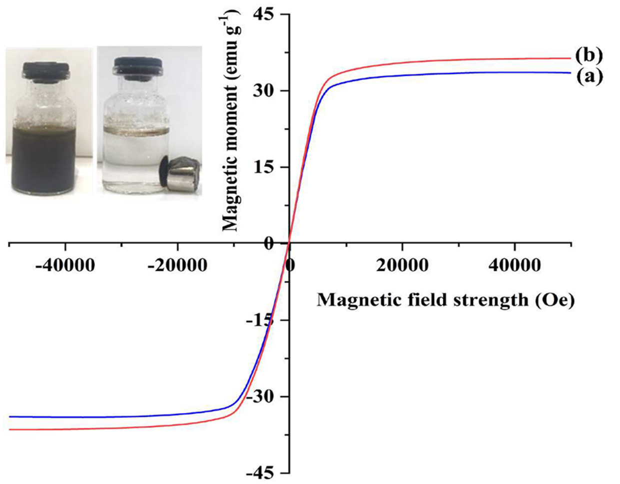

Figure 6. Magnetization curves of (a) Fe_3O_4-OA and (b) magnetic Fe_3O_4/SiO_2-NH_2 nanoparticles. The inset shows digital photographs of the magnetic separation of Fe_3O_4/SiO_2-NH_2 particles under external magnetic field from aqueous medium.

3.4. Thermal Stability of Fe_3O_4/SiO_2-NH_2 Nanoparticles. The thermal stabilities of magnetic Fe_3O_4/SiO_2-NH_2 and reference Fe_3O_4-OA nanoparticles are shown in Figure 7. The first weight loss for both magnetite nanoparticles at 100 °C is most likely due to the presence of loosely bounded and physiosorbed water.[69] The thermogram for Fe_3O_4-OA nanoparticles (Figure 7a) shows significant weight loss between 180 and 430 °C, which can be ascribable to the pyrolysis of organic content (OA), a clear indication of Fe_3O_4 surface coverage.[70] The organic material was thermally decomposed up to 450 °C, and the final residual weight of 70% represented the sample's inorganic iron oxide component.[71] The TGA curve (Figure 7b) of Fe_3O_4/SiO_2-NH_2 had also shown two-step weight loss. The elimination of surface adsorbed water molecules, and physically adsorbed solvent molecules trapped in the SiO_2 layer is responsible for the initial weight loss (4.3%) at temperatures ranging from 40 to 260 °C.[72] The second weight loss (4.4%) in the TGA curve at 260−480 °C is due to the disintegration of the aminopropyl moieties of APTES linked to the silica surface of the core Fe_3O_4.[73] In addition, for both samples a slight weight variation noticed at the temperature region of 600−784 °C is attributed to the phase transition from Fe_3O_4 to Fe_2O_3 and FeO structures.[74,75]

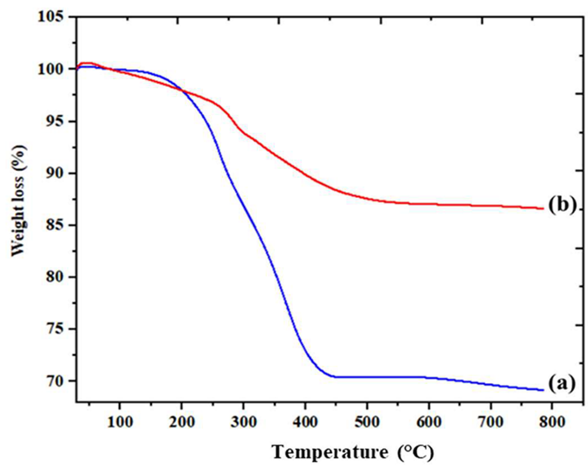

Figure 7. Thermograms of (a) Fe_3O_4-OA and (b) magnetic Fe_3O_4/SiO_2-NH_2 nanoparticles. Conditions: heating rate was 10 °C min^{-1}, under purging N_2.

3.5. pH-Responsive Surface Charge Potentials and Activities of Fe_3O_4/SiO_2-NH_2 Nanoparticles. The pH-dependent zeta potentials of Fe_3O_4-OA and Fe_3O_4/SiO_2-NH_2

https://doi.org/10.1021/acsomega.3c10082
ACS Omega 2024, 9, 20891−20905

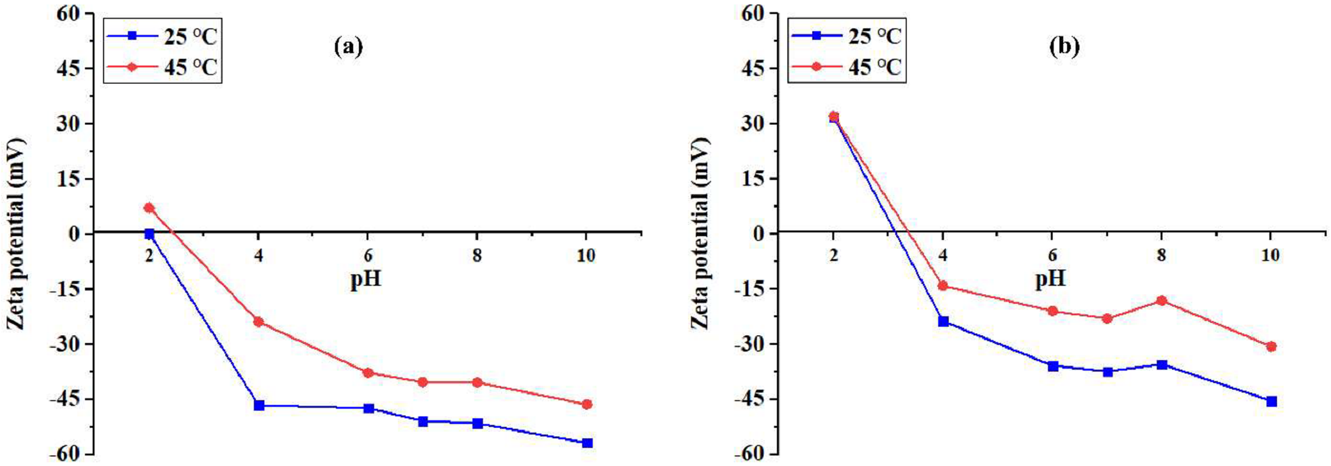

Figure 8. pH-dependent zeta potentials of Fe_3O_4-OA (a) and Fe_3O_4/SiO_2-NH_2 (b) at 25 and 40 °C.

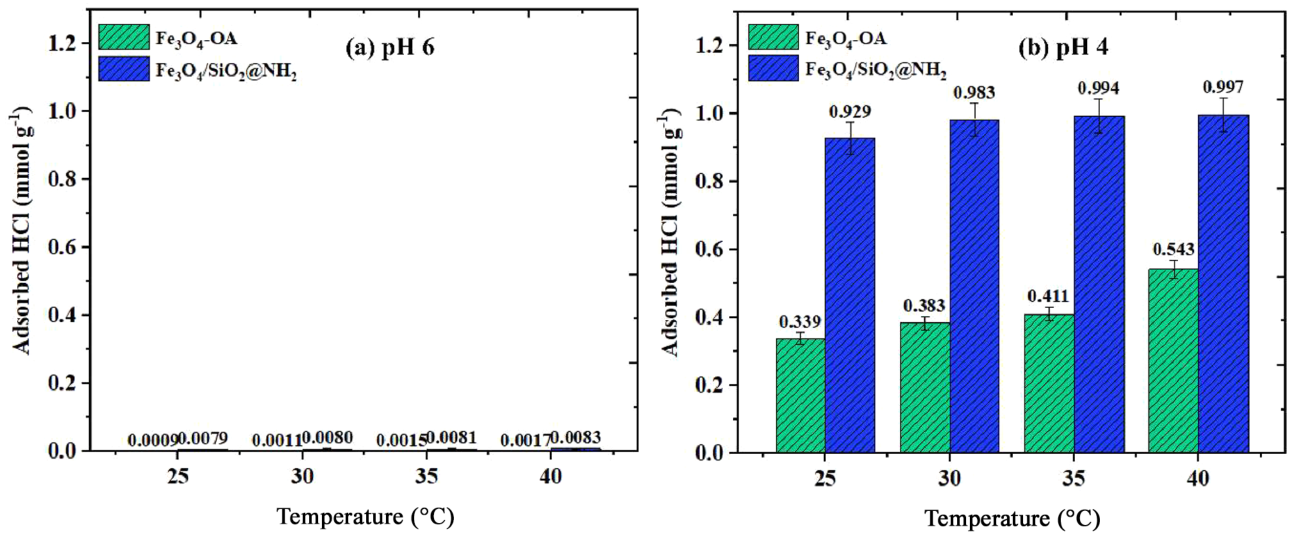

Figure 9. pH- and temperature-dependent capturing of protons onto the active surface of magnetic Fe_3O_4/SiO_2-NH_2 and reference-Fe_3O_4-OA nanoparticles: at pH 6 (a) and pH 4 (b) measured by a simple pH meter in distilled deionized water.

were measured in deionized distilled water at 25 and 40 °C, and the data are shown in Figure 8a and b. The negative charges on the Fe_3O_4-OA particles (Figure 8a) increased with increasing pH, which is plausibly due to the protonation of free hydroxyl groups at higher pH values. The zeta potential of Fe_3O_4-OA showed higher positive values in the range of pH 4−10 at 40 °C than that at 25 °C, which indicates that the zeta values were slightly increased with increasing temperature.[76] At pH 2, zeta potential values were slightly raised up to 0.3 mV to 7.2 mV at 25 and 40 °C, respectively. The variations of the zeta potential of Fe_3O_4/SiO_2-NH_2 nanoparticles (Figure 8b) showed that as pH is increased from 4 to 10, the negative charge density gradually increased. Fe_3O_4/SiO_2-NH_2 nanoparticles appeared to have a higher positive zeta potential at pH 2, which is ascribable to the protonation of amine groups and free -OH groups present on the surface of particles in aqueous dispersion. Hence, the amount of positive charge on the surface of Fe_3O_4/SiO_2-NH_2 particles is obviously higher than that on the Fe_3O_4-OA particles.[67,77] The point zero surface charge values of Fe_3O_4-OA and Fe_3O_4/SiO_2-NH_2 were found to be about 2.0 and 3.1 at 25 °C; and 2.5 and 3.4 at 40 °C, respectively. The significant changes in zeta potential values as well as the change of point zero charge values at a higher extent is the clear indication of surface modification with aminated silica.

3.6. pH- and Temperature-Dependent Proton Capturing of Fe_3O_4/SiO_2-NH_2 Nanoparticles. Figure 9 shows the pH- and temperature-dependent proton capturing amounts for the active surface of Fe_3O_4/SiO_2-NH_2 and reference Fe_3O_4-OA nanoparticles. Regardless of the temperature rises, both the reference Fe_3O_4-OA and Fe_3O_4/SiO_2-NH_2 magnetic nanoparticles exhibited quite minimal proton capturing activities (Figure 9a), which was attributed to the least availability of protons in the dispersion medium at pH 6. However, the proton capturing activities for both particles were significantly increased with increasing temperatures at pH 4. The proton capture efficiency for Fe_3O_4/SiO_2-NH_2 nanoparticles was almost double than that of reference Fe_3O_4-OA nanoparticles at each considered temperature (Figure 9b). This increasing tendency is due to the effective capturing of protons by amine, carboxylate, and hydroxyl groups present on the active surface of Fe_3O_4/SiO_2-NH_2 nanoparticles. This clear distinction in capturing protons is plausibly due to the greater basicity of the -NH_2 groups present on the surface of Fe_3O_4/SiO_2-NH_2 nanoparticles than that of reference Fe_3O_4-OA material, which only has carboxylate and -OH groups. It is obvious

https://doi.org/10.1021/acsomega.3c10082
ACS Omega 2024, 9, 20891−20905

that at pH 4, more protons are available than at pH 6. At higher temperature the individual particles' vibrational motions have been increased, resulting in enhanced kinetic energy as well as higher entropy and more breakdown of entanglements and hydrogen bonding among active functional moieties with solvent present on the surface of each particles. Therefore, the enhanced density of active functional groups, namely hydroxyl, carboxylate, and amine, actively participated for effective capturing of protons.[78] The proton capturing activity reached a saturation point (0.997 mmol g^{-1}) for Fe_3O_4/SiO_2-NH_2 magnetic nanoparticles just after 35 min of incubation under 40 °C.

3.7. Adsorption of Aqueous CO_2 Gas by Magnetic Adsorbent Nanoparticles. The CO_2 adsorption efficiencies of Fe_3O_4/SiO_2-NH_2 and reference Fe_3O_4-OA magnetic particles at different temperatures, namely 25 °C, 30 °C, 35 °C, and 40 °C, are shown in Figure 10, and pH changes due to the adsorption of CO_2 are depicted in Figure S4. The bar chart (Figure 10) clearly indicates that Fe_3O_4/SiO_2-NH_2 magnetic nanoparticles consistently outperformed Fe_3O_4-OA magnetic nanoparticles at all temperatures. The adsorption amount of CO_2 by Fe_3O_4/SiO_2-NH_2 magnetic particles was minimum (0.799 mmol g^{-1}) at 25 °C, whereas at 40 °C, it was increased considerably to 0.921 mmol g^{-1}. On the contrary, reference Fe_3O_4-OA magnetic nanoparticles captured only 0.339 mmol g^{-1} of CO_2 at 25 °C, which increased slightly to 0.443 mmol g^{-1} at 40 °C. The larger amount of CO_2 capture by amine-functionalized magnetic nanoparticles is associated with the densely packed hydroxy groups and higher proton affinity toward the more basic amine groups[79,80] than those of the less basic hydroxyl and carboxy groups on Fe_3O_4-OA particles. In addition, the adsorption efficiency (%) of Fe_3O_4/SiO_2-NH_2 magnetic nanoparticles was also higher than that of the reference magnetic nanoparticles. Each measurement is done in triplicate under identical conditions, and averaged values are reported with standard error bars.

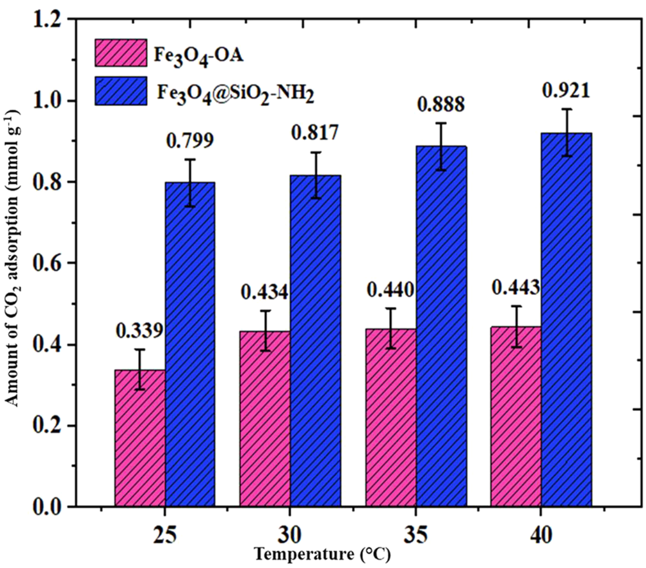

Figure 10. Amount of adsorption of CO_2 at different temperatures by reference-Fe_3O_4-OA and magnetic Fe_3O_4/SiO_2-NH_2 nanoparticles (conditions: stirring rate 100 rpm, dosage 0.01 g, time 6 h, and 100 mL water).

3.8. Plausible Mechanism for Aqueous CO_2 Gas Adsorption. The adsorption of CO_2 gas by synthesized Fe_3O_4/SiO_2-NH_2 and Fe_3O_4-OA nanoparticles involved a complex interplay of various forces and interactions, which is schematically depicted in Figure 11 and Figure S5, respectively.

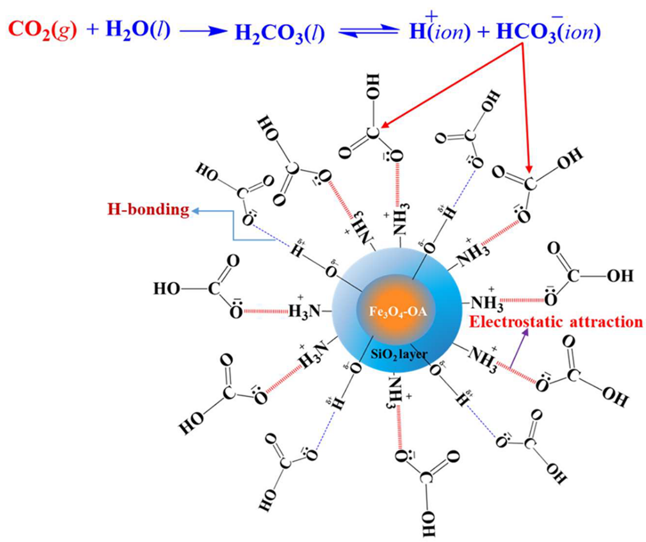

Figure 11. Plausible mechanism for aqueous CO_2 adsorption by magnetic Fe_3O_4/SiO_2-NH_2 nanoparticles.

First, due to the acidic nature of CO_2 gas, the passage of CO_2 gas molecules in H_2O produced H_2CO_3, which subsequently dissociated into H^+ and HCO_3^- ions. Second, the primary amine groups became positively charged (NH_3^+) by accepting such H^+ from the aqueous medium and electrostatic attraction and hydrogen bonding contributed to the adsorption of aqueous CO_2. For example, the positively charged -NH_3^+ ions on the Fe_3O_4/SiO_2-NH_2 magnetic particles interacted strongly with negatively charged HCO_3^- ions through electrostatic attraction forces, which is augmented the bicarbonate ions adsorption process. In addition, hydrogen bonding also played a crucial role for enhanced adsorption of aqueous CO_2. For instance, HCO_3^- ions contain polar bonds between oxygen and carbon, which can form hydrogen bonds with polar hydrogen-containing groups on the particle surfaces, like -NH_2, -COOH, or -OH. These bondings have stabilized the HCO_3^- ions on the surface of the magnetic nanoparticles. These interaction mechanisms work together to enhance the adsorption of CO_2, which is making these particles a promising candidate for carbon adsorption and storage applications in combating climate change and reducing greenhouse gas emissions.

An overview of the previous research on the adsorption of CO_2 by various adsorbent materials is shown in Table 1. Notably, our designed amine functional SiO_2 coated magnetic nanoparticles exhibited remarkable performance, demonstrating a significantly higher amount of CO_2 uptake compared to other magnetic particles. Furthermore, our nanoparticles showed an impressive adsorption percentage compared to the reported efficacy for CO_2 capturing. This exceptional performance is particularly noteworthy and due to the consideration of water as a CO_2 adsorption medium, which is also a sustainable and readily available green solvent. These findings demonstrated the potential of our designed magnetic particles as a promising candidate for CO_2 capturing and

https://doi.org/10.1021/acsomega.3c10082
ACS Omega 2024, 9, 20891−20905

Table 1. A Brief Overview of the Previous Research on the Adsorption of CO_2 by Different Adsorbent Materials

Researcher	Adsorbent Material	Uptake CO_2 (mmol g^{-1})	Absorption capacity (%)	Solvent type	T (K)	Refs
Muhyminul et al.	**Fe_2O_3-OA (0.01g)**	**0.44**	**47.52**	**Water**	**313**	**This work**
	Fe_3O_4/SiO_2-NH_2 (0.01g)	**0.92**	**90.00**			
Elhambakhsh et al. (2021)	Fe_2O_3 (0.025 wt %)	0.89	9.14	NMP	/	81
	Fe_2O_3-glutamine (0.5 wt %)	1.01	19.41			
Elhambakhsh and Keshavarz (2021)	Fe_3O_4	/	2.91	Sulfinol	308	37
	Fe_3O_4-proline		4.79			
	Fe_3O_4-lysine		6.3			
	$Fe_3O_4@SiO_2$-NH_2 (0.02 wt %)		13.36			
Zandavi et al. (2021)	Fe_3O_4 (0.03 wt %)	/	14	Low salinity water	333	82
	Fe_3O_4-PVA (0.11 wt %)		20.2			
	Fe_3O_4-PAM (0.11 wt %)		23.3			
Elhambakhsh et al. (2020)	Fe_3O_4 (0.1 wt %)	/	5.48	MDEA	308	71
	Fe_3O_4-proline (0.1 wt %)		6.78			
	Fe_3O_4-lysine (0.1 wt %)		12.39			
	$Fe_3O_4@SiO_2$-NH_2 (0.1 wt %)		16.38			
A. Hafizi et al. (2020)	DETA@ECH@Fe_3O_4 (0.5 wt %)	/	77.3	Water	293.15	38
Elhambakhsh et al. (2020)	Fe_3O_4 (0.1 wt %)	/	18	Water	308	83
	Fe_3O_4-proline (0.1 wt %)		24.18			
	Fe_3O_4-lysine (0.1 wt %)		27.14			
	$Fe_3O_4@SiO_2$-NH_2 (0.1 wt %)		31.18			
Elhambakhsh et al. (2020)	Fe_3O_4 (0.125 wt %)	/	18.12	Water	/	36
	Fe_3O_4-AP (0.125 wt %)		39.61			
	Fe_3O_4-lysine (0.125 wt %)		55.20			
	$Fe_3O_4@SiO_2$-AP (0.125 wt %)		78.00			
	$Fe_3O_4@SiO_2$-lysine (0.125 wt %)		88.00			
Arshadi et al. (2019)	$Fe_3O_4@SiO_2$-NH_2 (0.4 wt %)	/	70	Water	298	24
Aghehrochaboki et al. (2019)	GO (0.1 wt %)	/	9.1	MDEA	/	84
	GO (0.2 wt %)		10.14			
	PEI-GO (0.1 wt %)		15			
Haghtalab et al. (2015)	SiO_2 (0.1 wt %)	/	7	Water	278	85,32
Wei et al. (2020)	Dimethylaminopropylamine Ethyl 2,4-dichlorooxyaceta	2.440	/	/	303	86
Azmi et.al. (2020)	APTMS-MCN	0.010	/	/	298	87
Rahimi et al. (2019)	10 wt % MDEA + 5 wt % MEA-0.05 wt % nMWCNTs	0.738	/	MDEA	303	88
Rahmatmand et al. (2016)	Carbon nanotube (0.02 wt %)		34	MDEA	308	35
	Fe_3O_4 (0.02 wt %)		24			
N. H. Khdary et.al (2017)	PVDF-HFP-AFS 40 wt % SiO_2	0.767	/	/	/	89
S. Loganathan et al. (2016)	APTES MCM-41	0.00404	/	/	298	90

mitigation, surpassing the performance benchmarks set by previously studied adsorbents. Furthermore, use of recyclable and readily separable magnetic particles would help prevent mass loss and pressure drop as caused by nonmagnetic adsorbents in industrial packed columns.

3.9. Efficiency for CO_2 Adsorption of the Magnetically Recovered and Recycled Fe_3O_4/SiO_2-NH_2 Nanoparticles. Regeneration and reusability of adsorbent materials is paramount in a recyclable and easily accessible CO_2 adsorption process. Carbon capture processes in industrial settings often require such materials that can endure repetitive adsorption and regeneration steps. Figure 12 shows the adsorption efficacy of the recycled adsorbent particles. The adsorption efficiency for Fe_3O_4/SiO_2-NH_2 magnetic nanoparticles was 92.9%. However, this efficiency was slightly decreased with increasing number of cycles, as the active sites of adsorbent might be affected by the multiple treatments of magnetic fields as well as alkali treatments. Fe_3O_4/SiO_2-NH_2 magnetic nanoparticles almost retained their adsorption potentials, with only a 16.9% loss up to the fifth cycle. This observation is highly

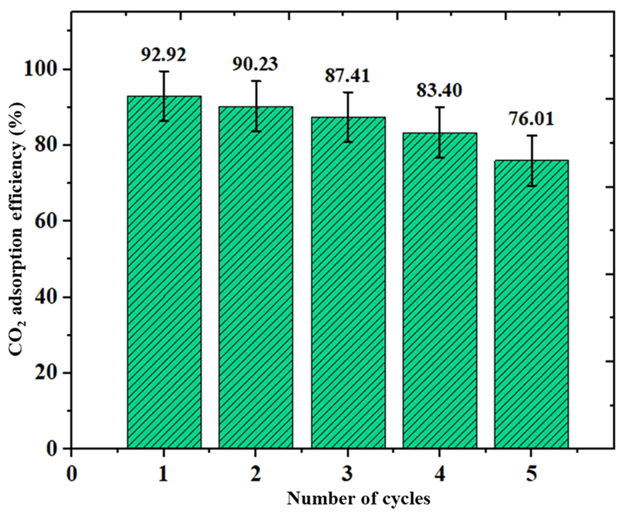

Figure 12. Adsorption efficiencies of magnetically recycled-$Fe_3O_4@SiO_2$-NH_2 nanoparticles for aqueous CO_2.

https://doi.org/10.1021/acsomega.3c10082
ACS Omega 2024, 9, 20891−20905

encouraging and underscores the robustness and longevity of these nanoparticles as an effective adsorbent for CO_2. The reusability of these nanoparticles not only reduces the environmental footprint of carbon adsorption processes but also offers economic advantages by lowering the need for frequent replacement of adsorbent materials.

4. CONCLUSIONS

Amine-functional silica coated magnetic Fe_3O_4/SiO_2-NH_2 nanoparticles were successfully synthesized and characterized using various analytical techniques, such as FTIR, TGA, TEM, HRTEM, VSM, XRD, zeta potential, and DLS measurements. The obtained data ensured the formation and surface modification of magnetic nanoparticles with aminated silica moieties with desired properties for targeted applications like an efficient adsorbent for aqueous CO_2 gas adsorption. Before CO_2 adsorption, the particles were investigated as an adsorbent for adsorbing protons from aqueous medium at pH 4 and 6. The nanoadsorbent particles showed good proton capturing efficiencies, and they must have promising capabilities for CO_2 capture due to the presence of basic amino groups. At 40 °C, they demonstrated remarkable efficiency by capturing up to 92.9% of CO_2 from water, with a minimal adsorbent dosage of 0.01 g. Notably, these findings were obtained in a simple single-plant setup; in our future report we may highlight the potential for further enhancement in a multiplant setup, which would help to achieve almost 100% adsorption of aqueous CO_2. This research warrants exploration in future investigation endeavors regarding the purification and management of acidic wastewater for both industrial and portable device design. The obtained results collectively demonstrated a promising, greener, and economically viable procedure for CO_2 adsorption and wastewater treatments. Furthermore, it stands out as an environmentally friendly approach, as it generates nontoxic byproducts, such as solid $NaHCO_3$ formed from the gaseous effluent, and it did not necessitate any expensive chemicals, specially designed devices, or solvents. The designed material and developed process is cost-effective, atmospheric, and ecofriendly in nature, making it a commendable choice for aqueous CO_2 adsorption.

■ ASSOCIATED CONTENT

Supporting Information

The Supporting Information is available free of charge at https://pubs.acs.org/doi/10.1021/acsomega.3c10082.

> Optimization of the reaction conditions for the synthesis of Fe_3O_4/SiO_2-NH_2, pH changes during proton capturing activities of Fe_3O_4/SiO_2-NH_2 and reference-Fe_3O_4-OA magnetic nanoparticles, visualization of the experimental setup for the aqueous CO_2 adsorption process, adsorbent dosage effect on the efficiency for aqueous CO_2 adsorption, efficiency of CO_2 gas uptake by Fe_3O_4-OA in an aqueous medium, observable pH changes during the adsorption of aqueous CO_2 gas by Fe_3O_4/SiO_2-NH_2 and reference-Fe_3O_4-OA (PDF)

■ AUTHOR INFORMATION

Corresponding Authors

Md. Abdur Rahman − *Polymer Colloids and Nanomaterials Research Lab, Department of Chemistry, Faculty of Science, University of Rajshahi, Rajshahi 6205, Bangladesh;* orcid.org/0000-0002-3855-8160; Email: arahman@ru.ac.bd

Md. Ashraful Alam − *Polymer Colloids and Nanomaterials Research Lab, Department of Chemistry, Faculty of Science, University of Rajshahi, Rajshahi 6205, Bangladesh;* Email: aashraful41@ru.ac.bd

Authors

Md. Muhyminul Islam − *Polymer Colloids and Nanomaterials Research Lab, Department of Chemistry, Faculty of Science, University of Rajshahi, Rajshahi 6205, Bangladesh*

Md. Mahbubor Rahman − *Polymer Colloids and Nanomaterials Research Lab, Department of Chemistry, Faculty of Science, University of Rajshahi, Rajshahi 6205, Bangladesh;* orcid.org/0000-0002-6763-525X

O. Thompson Mefford − *Department of Materials Science and Engineering, Clemson University, Clemson, South Carolina 29634-0971, United States;* orcid.org/0000-0002-9164-2521

Anwar Ul-Hamid − *Core Research Facilities, King Fahd University of Petroleum and Minerals, 31261 Dhahran, Saudi Arabia;* orcid.org/0000-0002-0259-301X

Jalil Miah − *Polymer Colloids and Nanomaterials Research Lab, Department of Chemistry, Faculty of Science, University of Rajshahi, Rajshahi 6205, Bangladesh*

Hasan Ahmad − *Polymer Colloids and Nanomaterials Research Lab, Department of Chemistry, Faculty of Science, University of Rajshahi, Rajshahi 6205, Bangladesh;* orcid.org/0000-0003-1499-167X

Complete contact information is available at: https://pubs.acs.org/10.1021/acsomega.3c10082

Notes

The authors declare no competing financial interest.

■ ACKNOWLEDGMENTS

We gratefully acknowledge the Materials Science Division, Atomic Energy Centre, Dhaka-1000, for assistance regarding the X-ray diffraction measurement. Md. Muhyminul Islam is pleased to convey his gratitude to the Ministry of Science and Technology of Bangladesh for providing him a National Science and Technology fellowship during his M.Sc. research. We are grateful for the supports regarding FTIR and TGA measurements from the Central Science Laboratory of the University of Rajshahi. The authors from RU thankfully acknowledge the financial support from the Faculty of Science, University of Rajshahi.

■ REFERENCES

(1) Lee, J. W.; Pineda, I. T.; Lee, J. H.; Kang, Y. T. Combined CO_2 absorption/regeneration performance enhancement by using nano-absorbents. *Applied Energy* **2016**, *178*, 164−176.

(2) Intergovernmental Panel on Climate Change (IPCC); Delmotte, V. M.; Zhai, P.; Pörtner, H.-O.; Roberts, D.; Skea, J.; Shukla, P. R.; Pirani, A.; Moufouma-Okia, W.; Péan, C.; Pidcock, R.; Connors, S.; Matthews, J. B. R.; Chen, Y.; Zhou, X.; Gomis, M. I.; Lonnoy, E.; Maycock, T.; Tignor, M.; Waterfield, T. Global Warming of 1.5°C. *IPCC Special Report on the Impacts of Global Warming of 1.5°C above Pre-industrial Levels and Related Global Greenhouse Gas Emission Pathways, in the Context of Strengthening the Global Response to the Threat of Climate Change, Sustainable Development, and Efforts to Eradicate Poverty* **2018**, 49−92.

(3) Cai, Y.; Yue, X.; Zhou, X.; Ren, Z.; Wei, Y.; Pan, Y. Simulated long-term evolution of the thermosphere during the Holocene-Part 1: Neutral density and temperature. *Atmospheric Chemistry and Physics* **2023**, *23*, 5009−5021.

(4) Munday, P. L.; Crawley, N. E.; Nilsson, G. E. Interacting effects of elevated temperature and ocean acidification on the aerobic performance of coral reef fishes. *Mar. Ecol.: Prog. Ser.* **2009**, *388*, 235−242.

(5) Frommel, A.; Maneja, R.; Lowe, D.; Malzahn, A.; Geffen, A.; Folkvord; Piatkowski, U.; Clemmesen, C. Severe tissue damage in Atlantic cod larvae under increasing ocean acidification. *Nature Climate Change* **2012**, *2*, 42−46.

(6) Groysman, A. Corrosion problems and solutions in oil, gas, refining and petrochemical industry. *Koroze an ochrana material* **2017**, *61* (3), 100−117.

(7) Stewart, C.; Hessami, M. A. A study of methods of carbon dioxide capture and sequestration- The sustainability of a photosynthetic bioreactor approach. *Energy Conversion and Management* **2005**, *46*, 403−20.

(8) Rashidi, N. A.; Yusup, S. An overview of activated carbons utilization for the postcombustion carbon dioxide capture. *Journal of CO_2 Utilization* **2016**, *13*, 1−16.

(9) Zheng, L. Overview of oxy-fuel combustion technology for carbon dioxide (CO_2) capture. *Woodhead Publishing* **2011**, 1−13.

(10) Dillon, D. J.; Panesar, R. S.; Wall, R. A.; Allam, R. J.; White, V.; Gibbins, J.; Haines, M. R. Oxy-combustion processes for CO_2 capture from power plant. *Greenhouse Gas Control Technologies* **2005**, *I*, 211−220.

(11) Singh, N.; Farina, I.; Petrillo, A.; Colangelo, F.; De Felice, F. Carbon capture, sequestration, and usage for clean and green environment: challenges and opportunities. *International Journal of Sustainable Engineering* **2023**, *16* (1), 248−268.

(12) Kenarsari, S. D.; Yang, D.; Jiang, G.; Zhang, S.; Wang, J.; Russell, A. G. Review of recent advances in carbon dioxide separation and capture. *Royal Society of Chemistry Advances* **2013**, *3*, 22739.

(13) Kim, Y. E.; Moon, S. J.; Yoon, Y., II; Jeong, S. K.; Park, K. T.; Bae, S. T. Heat of absorption and absorption capacity of CO_2 in aqueous solutions of amine containing multiple amino groups. *Sep. Purif. Technol.* **2014**, *122*, 112−8.

(14) Lee, A. S.; Eslick, J. C.; Miller, D. C.; Kitchin, J. R. Comparisons of amine solvents for postcombustion CO_2 capture: A multi-objective analysis approach. *International Journal of Greenhouse Gas Control* **2013**, *18*, 68−74.

(15) Kim, D. H.; Park, M. S.; Kim, N. U.; Ryu, D. Y.; Kim, J. H. Multifunctional amine-containing PVA-g-POEM graft copolymer membranes for CO_2 capture. *Macromolecules* **2018**, *51* (15), 5646−5655.

(16) Zhang, X.; He, X.; Gundersen, T. Post-combustion carbon capture with a gas separation membrane: parametric study, capture cost, and exergy analysis. *Energy Fuels* **2013**, *27*, 4137−49.

(17) Khosrowshahi, M. S.; Mashhadimoslem, H.; Shayesteh, H.; Singh, G.; Khakpour, E.; Guan, X.; Rahimi, M.; Maleki, F.; Kumar, P.; Vinu, A. Natural Products Derived Porous Carbons for CO_2 Capture. *Advanced Science* **2023**, *10*, 2304289.

(18) Lee, S. Y.; Park, S. J. A review on solid adsorbents for carbon dioxide capture. *Journal of Industrial and Engineering Chemistry* **2015**, *23*, 1−11.

(19) Sharma, H.; Dhir, A. Capture of carbon dioxide using solid carbonaceous and non-carbonaceous adsorbents: a review. *Environmental Chemistry Letters* **2021**, *19*, 851−873.

(20) Lin, P. H.; Wong, D. S. H. Carbon dioxide capture and regeneration with amine/alcohol/water blends. *International Journal of Greenhouse Gas Control* **2014**, *26*, 69−75.

(21) Chowdhury, F. A.; Yamada, H.; Higashii, T.; Goto, K.; Onoda, M. CO_2 Capture by tertiary amine absorbents: A Performance Comparison Study. *Ind. Eng. Chem. Res.* **2013**, *52*, 8323−8331.

(22) Kim, Y. E.; Lim, J. A.; Jeong, S. K.; Yoon, Y., II; Bae, S. T.; Nam, S. C. Comparison of carbon dioxide absorption in aqueous MEA, DEA, TEA, and AMP solutions. *Bulletin of the Korean Chemical Society* **2013**, *34*, 783−787.

(23) Spigarelli, B. P.; Kawatra, S. K. Opportunities and challenges in carbon dioxide capture. *Journal of CO_2 Utilization* **2013**, *1*, 69−87.

(24) Arshadi, M.; Taghvaei, H.; Abdolmaleki, M.; Lee, M.; Eskandarloo, H.; Abbaspourrad, A. Carbon dioxide absorption in water/nanofluid by a symmetric amine-based nanodendritic adsorbent. *Applied Energy* **2019**, *242*, 1562−1572.

(25) Pineda, I. T.; Lee, J. W.; Jung, I.; Kang, Y. T. CO_2 absorption enhancement by methanol-based Al_2O_3 and SiO_2 nanofluids in a tray column absorber. *International Journal of Refrigeration* **2012**, *35*, 1402−1409.

(26) Kim, W.-g.; Kang, H. U.; Jung, K.-m.; Kim, S. H. Synthesis of silica nanofluid and application to CO_2 absorption. *Sep. Sci. Technol.* **2008**, *43* (11−12), 3036−3055.

(27) Salimi, J.; Salimi, F. CO_2 capture by water-based Al_2O_3 and Al_2O_3-SiO_2 mixture nanofluids in an absorption packed column. *Revista Mexicana de Ingeniería Química* **2016**, *15* (1), 185−192.

(28) Hedayatnasab, Z.; Abnisa, F.; Daud, W. M. A. W. Review on magnetic nanoparticles for magnetic nanofluid hyperthermia application. *Materials & Design* **2017**, *123*, 174−196.

(29) Darvanjooghi, M. H. K.; Pahlevaninezhad, M.; Abdollahi, A.; Davoodi, S. M. Investigation of the effect of magnetic field on mass transfer parameters of CO_2 absorption using Fe_3O_4-water nanofluid. *AIChE J.* **2017**, *63*, 2176−2186.

(30) Peyravi, A.; Keshavarz, P.; Mowla, D. Experimental investigation on the absorption enhancement of CO_2 by various nanofluids in hollow fiber membrane contactors. *Energy Fuels* **2015**, *29*, 8135−8142.

(31) Veawab, A.; Tontiwachwuthikul, P.; Chakma, A. Corrosion behavior of carbon steel in the CO_2 absorption process using aqueous amine solutions. *Ind. Eng. Chem. Res.* **1999**, *38*, 3917−3924.

(32) Haghtalab, A.; Mohammadi, M.; Fakhroueian, Z. Absorption and solubility measurement of CO_2 in water-based ZnO and SiO_2 nanofluids. *Fluid Phase Equilib.* **2015**, *392*, 33−42.

(33) Samadi, Z.; Haghshenasfard, M.; Moheb, A. CO_2 absorption using nanofluids in a wetted-wall column with external magnetic field. *Chem. Eng. Technol.* **2014**, *37* (3), 462−470.

(34) Salimi, J.; Haghshenasfard, M.; Etemad, S. G. CO_2 absorption in nanofluids in a randomly packed column equipped with magnetic field. *Heat and mass transfer* **2015**, *51* (5), 621−629.

(35) Rahmatmand, B.; Keshavarz, P.; Ayatollahi, S. Study of absorption enhancement of CO_2 by SiO_2, Al_2O_3, CNT, and Fe_3O_4 nanoparticles in water and amine solutions. *Journal of Chemical & Engineering Data* **2016**, *61*, 1378−1387.

(36) Elhambakhsh, A.; Zaeri, M. R.; Mehdipour, M.; Keshavarz, P. Synthesis of different modified magnetic nanoparticles for selective physical/chemical absorption of CO_2 in a bubble column reactor. *Journal of Environmental Chemical Engineering* **2020**, *8* (5), 104195.

(37) Elhambakhsh, A.; Keshavarz, P. Enhanced CO_2 capture efficiency applying amine-based nano magnetite/sulfinol-M nano solvents at high pressures. *Environmental Science and Pollution Research* **2021**, *28*, 3455−3464.

(38) Hafizi, A.; Rajabzadeh, M.; Khalifeh, R. Enhanced CO_2 absorption and desorption efficiency using DETA functionalized nanomagnetite/water nano-fluid. *Journal of Environmental Chemical Engineering* **2020**, *8* (4), 103845.

(39) Oddo, E.; Pesce, R. M.; Derudi, M.; Magagnin, L. Amino-functionalized magnetic nanoparticles for CO_2 capture. *International Journal of Smart and Nano Materials* **2021**, *12*, 472−490.

(40) Mahamud, M. A.; Galib, A S M M.; Islam, M. M.; Mahiuddin, M.; Rahman, M. A.; Rahman, M. M.; Islam, M. S.; Ahmad, H.; Alam, M. A. Capturing acidic CO_2 using surface active di-functional core-shell composite polymer particles via aqueous medium. *ACS Omega* **2023**, *8*, 44523.

(41) Izgi, M. S.; Ece, S.; Kazici, H. C.; Sahin, O.; Onat, E. Hydrogen production by using Ru nanoparticle decorated with Fe_3O_4@SiO_2-NH_2 core-shell microspheres. *Int. J. Hydrogen Energy* **2020**, *45*, 30415−30430.

https://doi.org/10.1021/acsomega.3c10082
ACS Omega 2024, 9, 20891−20905

(42) Veisi, H.; Ozturk, T.; Karmakar, B.; Tamoradi, T.; Hemmati, S. In situ decorated Pd NPs on chitosan-encapsulated Fe_3O_4/SiO_2-NH_2 as magnetic catalyst in Suzuki-Miyaura coupling and 4-nitrophenol reduction. *Carbohydr. Polym.* **2020**, *235*, 115966.
(43) Hwang, S. W.; Umar, A.; Dar, G. N.; Kim, S. H.; Badran, R. I. Synthesis and characterization of iron oxide nanoparticles for phenyl hydrazine sensor applications. *Sensor Letters* **2014**, *12*, 97.
(44) Nigam, B.; Prakash, S. A.; Satsangi, S.; Mahto, P. K.; Swain, B. P. Synthesis and characterization of Fe_3O_4 nanoparticles for nanofluid applications-A Review. *Materials Science and Engineering* **2018**, *377*, 012187.
(45) Lan, Q.; Liu, C.; Yang, F.; Liu, S.; Xu, J.; Sun, D. Synthesis of bilayer oleic acid-coated Fe_3O_4 nanoparticles and their application in pH-responsive Pickering emulsions. *J. Colloid Interface Sci.* **2007**, *310*, 260−269.
(46) Yuan, Q.; Chi, Y.; Yu, N.; Zhao, Y.; Yan, W.; Li, X.; Dong, B. Amino-functionalized magnetic mesoporous microspheres with good adsorption properties. *Mater. Res. Bull.* **2014**, *49*, 279−284.
(47) Rafiee, F.; Mehdizadeh, N. Palladium N-Heterocyclic Carbene complex of vitamin B1 supported on silica-coated Fe_3O_4 nanoparticles: A Green and Efficient Catalyst for C-C Coupling. *Catal. Lett.* **2018**, *148*, 1345−1354.
(48) Gubanov, A. I.; Churakova, E. M.; Badmaev, S. D.; Sytnikov, P. V.; Filatov, E. Y.; Plyusnin, P. E.; Kurat'eva, N. V.; Sobyanin, V. A.; Korneev, S. V. Synthesis of nanosize Co-Rh systems and study of their properties. *Russian Journal of Applied Chemistry* **2011**, *84* (10), 1677−1683.
(49) Aljarrah, M. T.; Al-Harahsheh, M. S.; Mayyas, M.; Alrebaki, M. In situ synthesis of quaternary ammonium on silica-coated magnetic nanoparticles and its application for the removal of uranium (VI) from aqueous media. *Journal of Environmental Chemical Engineering* **2018**, *6*, 5662−5669.
(50) Gemeay, A. H.; Keshta, B. E.; El-Sharkawy, R. G.; Zaki, A. B. Chemical insight into the adsorption of reactive wool dyes onto amine-functionalized magnetite/silica core-shell from industrial wastewaters. *Environmental Science and Pollution Research* **2020**, *27*, 32341−32358.
(51) Xu, J.; Ju, C.; Sheng, J.; Wang, F.; Zhang, Q.; Sun, G.; Sun, M. Synthesis and characterization of magnetic nanoparticles and its application in lipase immobilization. *Bulletin of the Korean Chemical Society* **2013**, *34*, 2408−2412.
(52) Salafranca, J.; Gazquez; Pérez, N.; Labarta, A.; Pantelides, S. T.; Pennycook, S. J.; Batlle, X.; Varela, M. Surfactant organic molecules restore magnetism in metal-oxide nanoparticle surfaces. *Nano Lett.* **2012**, *12*, 2499−2503.
(53) Nahar, Y.; Rahman, M. A.; Hossain, M. K.; Sharafat, M. K.; Karim, M. R.; Elaissari, A.; Ochiai, B.; Ahmad, H.; Rahman, M. M. A facile one-pot synthesis of poly (acrylic acid)-functionalized magnetic iron oxide nanoparticles for suppressing reactive oxygen species generation and adsorption of biocatalyst. *Materials Research Express* **2020**, *7*, 016102.
(54) Wang, C. Y.; Hong, J. M.; Chen, G.; Zhang, Y.; Gu, N. Facile method to synthesize oleic acid-capped magnetite nanoparticles. *Chinese Chemical Letters 21* **2010**, *21*, 179−182.
(55) Zhao, S. Y.; Don, K. L.; Chang, W. K.; Cha, H. G.; Kim, Y. H.; Kang, Yo. S. Synthesis of magnetic nanoparticles of $Fe_3O_4$and $CoFe_2O_4$ and their surface modification by surfactant adsorption. *Bulletin of the Korean Chemical Society* **2006**, *27*, 237−242.
(56) Chen, M.; Shen, H.; Li, X.; Ruan, J.; Yuan, W. Q. Magnetic fluids' stability improved by oleic acid bilayer-coated structure via one-pot synthesis. *Chemical Papers 70* **2016**, *70*, 1642−1648.
(57) Rashid, M.; Rabbi, M. A.; Ara, T.; Hossain, M. M.; Islam, M. S.; Elaissari, A.; Ahmad, H.; Rahman, M. M. Vancomycin conjugated iron oxide nanoparticles for magnetic targeting and efficient capture of Gram-positive and Gram-negative bacteria. *Royal Society of Chemistry Advances* **2021**, *11*, 36319.
(58) Wang, J.; Zheng, S.; Shao, Y.; Liu, J.; Xu, Z.; Zhu, D. Amino-functionalized $Fe_3O_4@SiO_2$ core-shell magnetic nanomaterial as a novel adsorbent for aqueous heavy metals removal. *J. Colloid Interface Sci.* **2010**, *349*, 293−299.
(59) Andrzejewski, B.ło.; Bednarski, W.; Kaźmierczak, M.łg.; Łapinski, A.; Pogorzelec-Glaser, K.; Hilczer, B.; Jurga, S.; Nowaczyk, G.; Załęski, K.; Matczak, M.ł; Łęska, B.ła.; Pankiewicz, R.ła.; Kępinski, L. Magnetization enhancement in magnetite nanoparticles capped with alginic acid. *Composites Part B: Engineering* **2014**, *64*, 147−154.
(60) Sethulakshmi, N.; Sooraj, V.; Sajeev, U. S.; Nair, S. S.; Narayanan, T. N.; Joy, L. K.; Joy, P. A.; Ajayan, P. M.; Anantharaman, M. R. Contact potential induced enhancement of magnetization in polyaniline coated nanomagnetic iron oxides by plasma polymerization. *Appl. Phys. Lett.* **2013**, *103*, 162414.
(61) Kayal, S.; Ramanujan, R. V. Doxorubicin loaded PVA coated iron oxide nanoparticles for targeted drug delivery. *Materials Science and Engineering* **2010**, *30*, 484−490.
(62) Araghi, S. H.; Entezari, M. H. Amino-functionalized silica magnetite nanoparticles for the simultaneous removal of pollutants from aqueous solution. *Appl. Surf. Sci.* **2015**, *333*, 68−77.
(63) Rahman, M. A.; Ochiai, B. A facile aqueous production of bisphosphonated-polyelectrolyte functionalized magnetite nanoparticles for pH-specific targeting of acidicbone cells. *Royal Society of Chemistry Advances* **2022**, *12*, 8043.
(64) Mol, B.; Beeran, A. E.; Jayaram, P. S.; Prakash, P.; Jayasree, R. S.; Thomas, S.; Chakrapani, B.; Anantharaman, M. R.; Bushiri, M. J. Radio frequency plasma assisted surface modification of Fe_3O_4 nanoparticles using polyaniline/polypyrrole for bioimaging and magnetic hyperthermia applications. *J. Mater. Sci.* **2021**, *32*, 108.
(65) Hossain, S.; Rahman, M. M.; Nahar, Y.; Rahman, A.; Sharafat, M. K.; Hossain, M.; Ochiai, B.; Elaissari, A.; Ahmad, H. A simple in situ synthesis of iron oxide magnetic nanoparticles embedded in thermosensitive polymer for DNA capture. *Materials Research Society* **2020**, *35*, 2441−2450.
(66) Patil, R. M.; Shete, P. B.; Thorat, N. D.; Otari, S. V.; Barick, K. C.; Prasad, A.; Ningthoujam, R. S. B.; Tiwalea, M.; Pawar, S. H. Non-aqueous to aqueous phase transfer of oleic acid coated iron oxide nanoparticles for hyperthermia application. *Royal Society of Chemistry Advances* **2014**, *4*, 4515.
(67) Jadhav, S. V.; Nikam, D. S.; Khot, V. M.; Thorat, N. D.; Phadatare, M. R.; Ningthoujam, R. S.; Salunkhe, A. B.; Pawar, S. H. Studies on colloidal stability of PVP-coated LSMO nanoparticles for magnetic fluid hyperthermia. *New J. Chem.* **2013**, *37*, 3121−3130.
(68) Lemine, O. M.; Alanazi, A.; Albert, E. L.; Hjiri, M.; M'hamed, M. O.; Alrub, S. A.; Alkaoud, A.; Abdullah, C. A. C. γ-Fe_2O_3/Gd_2O_3-chitosan magnetic nanocomposite for hyperthermia application: structural, magnetic, heating efficiency and cytotoxicity studies. *Appl. Phys. A: Mater. Sci. Process.* **2020**, *126*, 471.
(69) Debnath, M. K.; Rahman, A. R.; Tauer, K.; Minami, H.; Rahman, M. R.; Gafur, M. A.; Ahmad, H. Evaluating the performance of citric acid as stabilizer and doping agent in an environment friendly approach to prepare electromagnetic nanocomposite particles. *Polym. Compos.* **2018**, *39*, 4628.
(70) Bristy, S. S.; Rahman, M. R.; Tauer, K.; Minami, H.; Ahmad, H. Preparation and characterization of magnetic γ-Al_2O_3 ceramic nanocomposite particles with variable Fe_3O_4 content and modification with epoxide functional polymer. *Ceram. Int.* **2018**, *44*, 3951−3959.
(71) Baghshahi, S.; Yousefi, F. A new systematic approach to the morphology and magnetic properties of spherical, cubic, and rod-like magnetite nanoparticles. *Journal of Superconductivity and Novel Magnetism* **2021**, *34*, 1949−1954.
(72) Alterary, S. S.; AlKhamees, A. Synthesis, surface modification, and characterization of $Fe_3O_4@SiO_2$ core@shell nanostructure. *Green Processing and Synthesis* **2021**, *10*, 384−391.
(73) Sun, S.; Zeng, H.; Robinson, D. B.; Raoux, S.; Rice, P. M.; Wang, S. X.; Li, G. Monodisperse MFe_2O_4 (M) Fe, Co, Mn) nanoparticles. *J. Am. Chem. Soc.* **2004**, *126*, 273−279.
(74) Wu, D.; Zhao, J.; Cheng, J.; Liu, C.; Wang, Q. Laser shock fabrication of nitrogen doped inverse spinel Fe_3O_4/carbon nanosheet

film electrodes towards hydrogen evolution reactions in alkaline media. *International Journal of Molecular Sciences* **2022**, *23*, 7477.

(75) Mazo-Zuluaga, J.; Barrero, C. A.; Diaz-Teran, J.; Jerez, A. Thermally induced magnetite-haematite transformation. *Hyperfine Interact.* **2003**, *148/149*, 153−161.

(76) Nayeem, J.; Al-Bari, M. A. A.; Mahiuddin, M.; Rahman, M. A.; Mefford, O. T.; Ahmad, H.; Rahman, M. M. Silica coating of iron oxide magnetic nanoparticles by reverse microemulsion method and their functionalization with cationic polymer P(NIPAm-co-AMPTMA) for antibacterial vancomycin immobilization. *Colloids Surf., A* **2021**, *611*, 125857.

(77) Shete, P. B.; Patil, R. M.; Tiwale, B. M.; Pawar, S. H. Water dispersible oleic acid-coated Fe_3O_4 nanoparticles for biomedical applications. *J. Magn. Magn. Mater.* **2015**, *377*, 406−410.

(78) Sasabe, H.; Saito, S. Effects of temperature and pressure on the micro-Brownian motion in poly (vinyl chloride). *Polym. J.* **1972**, *3*, 631−639.

(79) Sundar, L. S.; Sharma, K. V.; Naik, M. T.; Singh, M. K. Empirical and theoretical correlations on viscosity of nanofluids: a review. *Renewable and Sustainable Energy Reviews* **2013**, *25*, 670−86.

(80) Jung, J.-Y.; Lee, J. W.; Kang, K. T. CO_2 absorption characteristics of nanoparticle suspensions in methanol. *Journal of Mechanical Science and Technology* **2012**, *26*, 2285−90.

(81) Elhambakhsh, A.; Heidari, S.; Keshavarz, P. Experimental study of carbon dioxide absorption by Fe_2O_3@glutamine/NMP nanofluid. *Environmental Science and Pollution Research* **2022**, *29*, 1060−1072.

(82) Zandahvifard, M. J.; Elhambakhsh, A.; Ghasemi, M. N.; Esmaeilzadeh, F.; Parsaei, R.; Keshavarz, P.; Wang, X. Effect of modified Fe_3O_4 magnetic NPs on the absorption capacity of CO_2 in water, wettability alteration of carbonate rock surface, and water-oil interfacial tension for oilfield applications. *Ind. Eng. Chem. Res.* **2021**, *60*, 3421−3434.

(83) Elhambakhsh, A.; Keshavarz, P. Investigation of carbon dioxide absorption using different functionalized Fe_3O_4 magnetic nanoparticles. *Energy Fuels* **2020**, *34*, 7198−7208.

(84) Aghehrochaboki, R.; Chaboki, Y. A.; Maleknia, S. A.; Irani, V. Polyethyleneimine functionalized graphene oxide/methyldiethanolamine nanofluid: Preparation, characterization, and investigation of CO_2 absorption. *Journal of Environmental Chemical Engineering* **2019**, *7*, 103285.

(85) Haghtalab, A.; Mohammadi, M.; Fakhroueian, Z. Absorption and solubility measurement of CO_2 in water-based ZnO and SiO_2 nanofluids. *Fluid Phase Equilib.* **2015**, *392*, 33−42.

(86) Chen, D.; Cheng, Y.; Zhou, N.; Chen, P.; Wang, Y.; Li, K.; Huo, S.; Cheng, P.; Peng, P.; Zhang, R.; Wang, L.; Liu, H.; Liu, Y.; Ruan, R. Photocatalytic degradation of organic pollutants using TiO_2-based photocatalysts: A review. *Journal of Cleaner Production* **2020**, *268*, 121725.

(87) Azmi, A. A.; Ruhaimi, A. H.; Aziz, M. A. A. Efficient 3-aminopropyltrimethoxysilane functionalised mesoporous ceria nanoparticles for CO_2 capture. *Materials Today Chemistry* **2020**, *16*, 100273.

(88) Rahimi, K.; Riahi, S.; Abbasi, M. Effect of host fluid and hydrophilicity of multi-walled carbon nanotubes on stability and CO_2 absorption of amine-based and water-based nanofluids. *Journal of Environmental Chemical Engineering* **2020**, *8*, 103580.

(89) Khdary, N. H.; Abdelsalam, M. E. Polymer-silica nanocomposite membranes for CO_2 capturing. *Arabian Journal of Chemistry* **2020**, *13*, 557−567.

(90) Loganathan, S.; Ghoshal, A. K. Amine tethered pore-expanded MCM-41: A promising adsorbent for CO_2 capture. *Chemical Engineering Journal* **2017**, *308*, 827−839.

https://doi.org/10.1021/acsomega.3c10082
ACS Omega 2024, 9, 20891−20905